sustainability

MDPI

Article

Evaluation of the Structural Performance of Low Carbon Concrete

Promise D. Nukah [1,*], Samuel J. Abbey [1], Colin A. Booth [2] and Jonathan Oti [3]

[1] School of Engineering, College of Arts, Technology and Environment, University of the West of England, Bristol BS16 1QY, UK
[2] Centre for Architecture and Built Environment Research (CABER), College of Arts, Technology and Environment, University of the West of England, Bristol BS16 1QY, UK
[3] School of Engineering, Faculty of Computing, Engineering and Science, University of South Wales, Pontypridd CF37 1DL, UK
* Correspondence: promise.nukah@uwe.ac.uk

Abstract: Evaluation of the effect of embodied carbon reduction using an optimized design section for a ground beam, use of supplementary cementitious materials, and replacement of normal aggregate with light weight aggregate on the mechanical properties of low-carbon concrete was carried out. A creep coefficient of 0.019 was estimated for a 365-day period on a change in section from 1 to 0.6 m^2 on a proposed trapezoidal section for ground beam, which showed a negligible difference when compared to the normal rectangular section owing to a reduction in embodied carbon due to the associated reduction in concrete volume and reinforcement. Training of 81 low-carbon concrete data sets in MATLAB using artificial neural network for 100% cement replacement with ground granular base slag indicates good performance with a mean square error of 0.856. From the study, it was observed that the extent of carbonation depth in concrete evidenced the measure of compressive strength formation based on the specific surface area of the binder and the water absorption rate of the aggregate, while enhancing the flexural strength of the low-carbon concrete required a cement-to-supplementary-cementitious-material ratio of 0.8.

Keywords: light weight aggregate; recycled aggregate; long-term deformation; cross-sectional area; concrete binder; artificial neutral network

Citation: Nukah, P.D.; Abbey, S.J.; Booth, C.A.; Oti, J. Evaluation of the Structural Performance of Low Carbon Concrete. *Sustainability* **2022**, *14*, 16765. https://doi.org/10.3390/su142416765

Academic Editor: José Ignacio Alvarez

Received: 3 November 2022
Accepted: 7 December 2022
Published: 14 December 2022

1. Introduction

Concrete is considered the most used building material on Earth after water, mainly because it is cost effective, constructable, durable, available, and attractive. It is a vital ingredient used to attain the United Nations Sustainable Development Goals in addressing affordable housing shortages, and it constitutes a major recipe for building infrastructure that affects 17 Sustainable Development Goals (SDG), including 121 of the 169 targets [1]. There have been increased cases of natural disasters such as earthquakes, for instance, which require a high resilient building made of concrete to minimize the impact of damage.

Cement is responsible for the compressive strength of concrete and is produced through a process that requires the heating of limestone and clay at a high temperature of about 1400 °C, which is associated with a high dissipation of carbon dioxide. Due to the mineralogy of the limestone as a primary material that is used in the production of cement, the product contains clinker, which is a high-carbon carrier in cement. It follows then that the carbon footprint of concrete, owing to the use of cement, constitutes immensely to the embodied carbon supply chain, with the cement industry being the second largest emitter of carbon dioxide (CO_2) [2]. Embodied carbon, which is the amount of carbon dioxide emitted to produce 1 kg of material, is one of the performance metrics to measure the environmental impact of a material. Quantitative sustainability assessment of concrete involves striking a balance and trade-offs based on performance, environmental impact, and cost.

Reducing the dosage of cement in concrete requires the use of alternative binders with pozzolanic and cementitious properties capable of with a near-zero effect on embodied carbon. Available alternative binders of waste materials include the use of calcined clay, ground granulated base slag (GGBS), pulverized fly ash (PFA), post-consumer glass and natural pozzolans.

In addition to the cement in concrete, aggregate contributes more than 60% by mass to the total weight of concrete and impacts the carbon footprint through the self-weight of the concrete structure and eventual increase in the amount of the required reinforcement [2]. Similarly, volume reduction of concrete through section optimization in reinforced concrete design is also a measure to reducing concrete-embodied carbon. The reduction of the carbon footprint of concrete through the replacement of the binder with supplementary cementitious material (SCM), use of recycled or light-weight aggregate (LWA) material, and the reduction in volume of concrete through an optimized section in design result in the production of a low-carbon concrete (LCC). It has been observed that while the LCC can mitigate the sustainability requirement, it requires an optimal mechanical performance in terms of compressive strength, flexural strength and improvement in creep and shrinkage as compared to the normal-weight concrete (NWC). Therefore, investigating the mechanical properties of LCC will directly impact on the choice of the materials and concrete mix proportion for an optimal structural performance.

This paper presents an evaluation of the most recent and related works analysing the mechanical properties of low-carbon concrete and investigating the possibility of complete replacement of cement with other sustainable pozzolanic materials for the concrete structural performance. The mechanical properties of concern in this study will include the concrete compressive strength, tensile strength, as well as creep and shrinkage. The use of a machine learning tool such as artificial neutral network (ANN) to investigate the structural performance of concrete at a complete cement replacement with GGBS is also considered in this paper.

2. Literature Review

The approach to reducing embodied carbon has either been finding the possibility of reducing cement content in concrete or complete replacement with sustainable pozzolanic materials. The results reported from the literature have not been without limitations in tensile strength, compressive strength, workability, and other properties that influence the structural behaviour of concrete. The preference for cement has mainly been for its high compressive strength with good mechanical behaviour to resist various degrees of loads and its acceptability for performance over the years. However, this acceptability has been tested on environmental impact, technical performance, and durability [3] and is found to be lacking in environmental sustainability due to the carbon emission factor. Concrete structural strength compared to its carbon emission using material volume reduction has been studied [4], with an evaluation on whether the replacement of cement as a concrete binder is realistic and the possibility for a reduction of concrete volume as a strategy to reducing embodied carbon in the construction industry.

Cement as a material component of concrete is a major carbon carrier which is recorded to account for about 3% of global annual carbon emission [5]. The use of limestone fillers, furnace slag, fly ash, and natural pozzolans as clinker are new developments in the cement production process, which portends a low impact in terms of carbon emission. As this available new development in cement production gains significant acceptance using new technologies, concrete mix design requires accuracy so that the high-carbon-intensive component of the mix can be reduced. This has been made possible with the use of waste solvent and biofuel, use of water-reducing admixtures and blending of supplementary cementitious material (SCM) in the production of Portland cement [6]. Similar improvement includes the partial replacement of clinker during cement production. The production of clinker involves the combination of about 80% of limestone and 20% of clay using blended additives and heated at about 1450 °C, which contributes to about 0.706 ton of CO_2 emission

during cement production. Studies have shown that the production of raw materials for the construction industry contributes to 93% of the total emissions, with 78% from concrete [7].

Crack formations in concrete are physical signs of its failure in terms of durability in response to its mechanical and structural performance. In describing the behaviour of concrete, design codes use the extent of exposure for concrete class in terms of the degree of its severity to describes its durability as a measure of expected performance throughout the design life of the structure. Studies carried out by [8] on the depth of carbonation for the lightweight aggregate concrete were found to be negligibly small.

The mix proportion of concrete materials as well as the materials used influence the durability of concrete. The durability of concrete is also likened to its deterioration state, hence the use of concrete additive to improve the internal pores of concrete to reducing the rate of water absorption to an optimal level as well as for crack control [9]. About 9% of water freezing in concrete is due to expansion of its pores, with concrete resistance to freezing likened to its permeability, degree of saturation, amount of water, and rate of freezing. The pressures developed in the concrete due to freezing include hydraulic and osmotic pressures which can form micro-cracks and will eventually lead to failure [10].

It is generally assumed that light-weight aggregate is not suitable for reinforced concrete work; however, it is proven that most light-weight aggregate can produce high strength depending on the type of binder, type of curing and type of aggregate used. Light-weight concrete has displayed significant advantages over normal-weight concrete. For example, the reduction in the structure's dead load consequently has a positive impact on the size of the foundation as well as the number of required reinforcements. This reduction in self weight has also make it very suitable for the construction of a large clear span structure. It has also been observed that there is an increased buoyancy when the lightweight concrete is submerged due to the reduction in density to an equivalent of 55% of dense concrete [11]. This makes it more susceptible for floating docks and offshore production platforms. Light-weight aggregate concrete offers a path for sustainable concrete as envisaged in the Environmental Product Declaration.

Environmental Product Declarations (EPDs) outline concrete mix design impact on the environment using global warming potentials (GWP) as an important metric of measurement of embodied carbon due to the global demand for concrete. The concern with low-carbon concrete due to weather and environmental variability includes early strength development, long-term performance, sustainability, and durability. To ascertain the improvement in reporting identifiable compliance of EPD, GWP is measured in $kgCO_2/m^3$ specific to a particular mix design in compliance with (BS) EN 15804:2012+A2:2019 [12] and to attain compliance with ultimate and serviceability limit state requirement.

The use of suitable SCM modifies the concrete matrix and its pore structure, which makes the LCC composites harden with high performances [13,14].

2.1. Compressive Strength

Concrete compressive strength measures the ability of the concrete to withstand applied load within the limit of tolerances as anticipated in the design. This depends on the concrete materials, mix proportion, curing condition, and age. The need for concrete that can minimize environmental burdens and meet the compressive strength requirements has aroused the interest of many. Studies have shown that cement cohesion occurs at the level of the nanoscale, which gives credence to the development of concrete strength with age for finer particle binders [15]; however, the prediction of its mechanical properties using physics-based models is challenging. Following the environmental challenges of cement and lack of definitive prediction model for its mechanical properties, researchers have resorted to making fair comparisons between extant and generated concrete mix in terms of the effect on the environment and optimal structural performance. There is also the tendency of the lightweight concrete to be less abrasive, which means that there will be a reduction in formwork during construction. Also observed is its better fire resistance and better insulating capabilities [16]. To achieve the desired concrete strength, the use of cement

and other pozzolanic materials in concrete formation for optimal compressive strength is attributed to the formation of a crystalline calcium silicate hydrate (C-S-H) [16,17]. The design and construction of low-carbon concrete using light-weight aggregate requires a new concrete formulation with reduced environmental impact and reduced embodied carbon without compromising strength. Concrete is usually identified by its density to characterize its stiffness which eventually define the compressive strength. The normal-weight concrete (NWC) is expressed in terms of density as a concrete of density ranging from 2240 to 2500 kg/m^3, whereas the lightweight concrete (LWC) ranges in density from 500 to 2000 kg/m^3. The properties of the LWC are determined by the aggregate materials that are naturally occurring or recycled. Examples of light-weight aggregate include expanded clay (LECA), expanded glass, volcanic pumice, and lytag.

LWC is affected by its high porous nature, which is greater than that of the normal aggregate because of the difference in porosity between the two; however, the rate of heat of hydration for early-age strength development for normal concrete is higher compared to the lightweight aggregate [18]. Due to the low density and porosity of the matrix of the LWC, there is significant reduction in strength at an early age [19]; however, there is potency in using recycled lightweight concrete aggregates (RLCA) as a constituent material for the LWC mix through an indication to increase the modulus of elasticity, compressive strength, and other mechanical properties of the LWC. The influence of aggregate size on the LWC is reported to significantly improve concrete performance as well as its behaviour. A study on a finite element modelling program of concrete on different aggregates with different sizing was conducted by Kurpińska and Ferenc [20] for LWC. Concrete compressive strength of 39.5–101 MPa was also achieved using expanded clay and fine expanded glass aggregate for different micro-fillers, including ground quartz sand and silica fume [21]. Regarding the properties of recycled aggregate, the mechanical properties of Lytag concrete were compared with the recycled aggregate mix of rubber mix at different replacement levels for sand. It was demonstrated that the compressive strength of the Lytag sample was found to be higher than rubber-sand-mixed concrete but exhibited low flexural bending resistance [22]. Normal-weight concrete (NWC) using coarse granite and sand was also compared with light-weight aggregate concrete (LWC) using lytag and sand in the study by Al-Allaf et al. [23]. A similar study by [24] on LWC using GGBS shows a decline in early strength which was mitigated with inclusion of metakaolin while a water to cementitious material ratio of 0.5 attains optimal compressive strength. The comparative mechanical properties for NWC and LWC are as presented in Table 1. It can be observed that it takes 192 kg of water to attain a compressive strength of 40 MPa for NWC, while it takes 216 kg of water for the LWC.

Table 1. Concrete Mechanical Properties.

Concrete Type	Cement, kg	Water, kg	Sand, kg	Coarse Aggregate, kg	Average Concrete Density, Kg/m^3	Average Concrete Strength MPa	% Compressive Strength Increase
NWC	400	192	667	1184	2345	41.6	1.5
LWC	480	216	485	715	1796	40.1	

In characterizing the compressive strength of concrete, one of the properties of concern in the concrete is the modulus of elasticity. The modulus of elasticity of concrete is referred to as the ratio of concrete compressive stress to corresponding strain both for tensile and compressive stresses within the elastic limit of the material. This can also be deduced from the stress–strain curve as the static modulus of elasticity taken as the slope of the secant [25].

From the result of mechanical properties of concrete according to [23], and as shown in Table 1, a 22.81% increase in the modulus of elasticity between the LWC and NWC resulted in about a 1.5% increase in compressive strength. The elastic property of a material is its ability to return to its original shape after deformation; hence, it can be argued that concrete

is not an elastic material because after failure, which is shown at concrete compressive testing, the original form is irrecoverable. This means then that the modulus of elasticity is a constant of non-linearity used as an approximation to describe concrete behaviour. This gives credence to the use of a rectangular parabolic curve in the determination of the concrete stress block as a parameter to deriving the design equation.

The modulus of elasticity has also been shown to depend on the aggregate properties as well as on the cement paste. While a higher size of aggregate may increase the porosity of the concrete, a finer coarse aggregate is likely to make the concrete denser, thereby increasing the modulus of elasticity. The modulus of elasticity of concrete is influenced by the concrete aggregate sizing which defines the concrete stiffness. At a lower age, the modulus of elasticity for GGBS and PFA was like that of NWC [25].

This means then that for low-carbon concrete (LCC) to be achieved, the aggregate sizing and the concrete strength must be considered. Several codes of practice take into consideration the density of concrete as a determination for the modulus of elasticity, for example, ACI 318 [26] provides the relation for the modulus of elasticity Ec as

$$Ec = 0.043wc^{1.5}\sqrt{fc}\ x\ 10^{-3}.\ \text{GPa}$$

where wc is the unit weight of concrete which varies between 1440 and 2560 kg/m^3 and fc is the compressive strength of concrete.

Similarly, Eurocode 2 [27] provides the modulus of elasticity as

$$Ec = 1.7wc^2\ \left(fc\right)^{1/3}\ \right)\ x\ 10^{-6}\ \text{GPa}$$

Studies have shown that LCC is preferably made of light-weight aggregate with a low density compared to NWC. Regarding concrete curing, steam curing of concrete is proven to accelerate the hydration reactions of Portland cement at atmospheric pressure. This improves the compressive strength, and the modulus of elasticity reduces concrete permeability in comparison with when the curing is performed under ambient conditions. Increasing the modulus of elasticity of LWC requires a reduction in the coarse aggregate sizing and the use of secondary cementitious materials with high pozzolanic activity [28,29].

2.2. Effect of Cross-Sectional Area

The analogy of finer coarse aggregate sizing for a higher modulus of elasticity can be explained from the mechanics of particle size interaction in the aggregate. The moment of inertia I of a rigid body in this case of aggregate is the property obtained by summing the product of the particle mass (expressed as area A) and the square of its distance y from a given axis ($\int\ y^2dA$). This is related to the moment of resistance M expressed as $M = \sigma Z$, where σ is the stress on the body and Z is the section modulus expressed as $Z = \frac{I}{y}$.

It follows that if y is higher than a certain value, z will be smaller; hence, the moment of resistance will be small relative to the stress on the body. Similarly, a smaller y versus a certain value will increase z, which will invariably increase M. An increase in the moment of resistance M improves the concrete strength when under load and often depends on the cross-sectional area A of the structure.

Considering the analysis of stress on a ground beam, the stress distribution pattern in soil on application of the load using the Boussinesq theory is seen to be trapezoidal, projecting at 45° from the top of the ground at the soil structure interface to the foundation [30]. With this stress pattern, the use of a trapezoidal section for the ground beam rather than the conventional rectangular section will result in concrete savings of 17.3 m^3 when comparing the section of same base width and height. Evaluating the creep coefficient with the control on the concrete cross-sectional area and age of concrete at loading, using parameters such as concrete characteristic strength (fck) of 40 MPa, concrete cross-sectional area (Ac = 1 m^2), part of the cross-section perimeter exposed to drying (U = 2), age of concrete at loading (to = 28 days), ambient temperature (T = 20 °C), relative humidity of ambient environment (RH = 70%), cement type (N), and age of concrete at the end of curing (t_0 = 365 days) from

the provision of Eurocode 2 [27], the variation of creep coefficient is shown in Tables 2–4 and Figure 1. It was observed that the creep coefficient at the cross-sectional area of 0.6 m^2 is 1.429 at 28 days of concrete loading, while at 365 days of concrete loading, it is 0.872.

Table 2. Creep coefficient variation with cross-sectional area.

Concrete Loading at 365 days		
Cross-sectional Area (m^2)	**Creep Coefficient**	**Shrinkage**
1	0.842	29.98
0.8	0.855	29.98
0.6	0.872	29.98
0.4	0.9	30.78
0.2	0.958	34.8

Table 3. Creep coefficient variation with cross-sectional area.

Concrete Loading at 56 days		
Cross-sectional Area (m^2)	**Creep Coefficient**	**SHRINKAGE**
1	1.209	29.98
0.8	1.227	29.98
0.6	1.252	29.98
0.4	1.293	30.78
0.2	1.375	34.8

Table 4. Creep coefficient variation with cross-sectional area.

Concrete Loading at 28 days		
Cross-sectional Area (m^2)	**Creep Coefficient**	**Shrinkage**
1	1.38	29.29
0.8	1.4	29.98
0.6	1.429	29.98
0.4	1.471	30.78
0.2	1.57	34.8

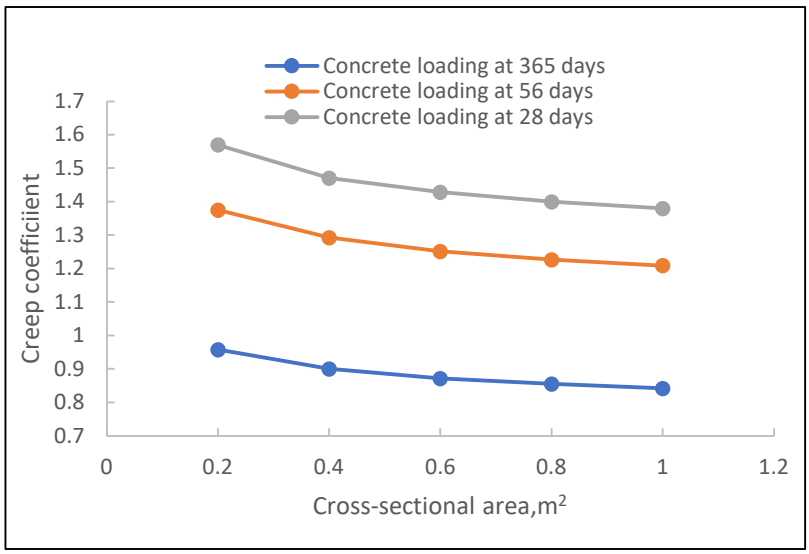

Figure 1. Creep coefficient with variation in cross-sectional area.

Similarly, the creep coefficient at the cross-sectional area of 1 m^2 is 1.38 at 28 days of concrete loading, while at 365 days for the same concrete loading, it is 0.842. For the 0.6 m^2,

there is a creep growth of 0.557 between 28 and 365 days for the same concrete loading, while for 1 m^2, it is 0.538. The difference in creep coefficient of 0.019 can be compensated through the reduction in concrete volume in terms of reduced embodied carbon, gain in material cost and overall impact on the environment.

The relationship of the mechanical properties of LWC has been studied by Young Sang Cho, Jeom Han Kim and Sung Uk Hong, [31] using ultrasonic pulse velocity (UPV). It was shown that the aggregate type in a mixture predicts the behaviour of the elastic modulus. The use of ultrasonic pulse velocity (UPV) as a non-destructive method was used by Hedjazi [32] to analyse the compressive strength of LWC. An expanded glass granule aggregate known as poraver was used in the study.

It has also been demonstrated that light-weight aggregate can replace normal-weight aggregate to achieve smaller bulk densities while UPV has been used as an alternative method for evaluation of compressive strength of LWC. Similarly, concrete workability is measured using the slump test as a measure of consistency, according to the European and British Standard. The slump class as described in [27] is useful in reducing the time for concrete placement from the point of production. In order words, low workability increases the cost of construction due to additional manpower that will be needed. In characterizing the strength of concrete, the usefulness of certain parameters predicts that the trend of behaviour in combination with the extent of confinement shows significant success. For instance, a greater static modulus of elasticity provides higher structural stiffness, which reduces mid-span deflection, especially for beams.

A study on the properties of blended low-calcium fly ash geopolymer concrete cured in ambient condition was conducted by Nath and Sarker [33]. The produced geopolymer concrete was produced using low-calcium fly ash with a small percentage of additives such as ground granulated blast furnace slag (GGBFS) and ordinary Portland cement (OPC). The mixed composition is shown in Table 5, and the compressive strength obtained is shown in Figure 2.

Table 5. Concrete mix composition for geopolymer concrete.

Mix Label	Coarse/Fine Aggregate	Fly ash	GGBS	Cement	Na_2SiO_3/NaOH
A40 S00	1.86	400	0		2.50
A40 S10	1.86	360	40		2.50
A40 S15	1.86	340	60		2.50
A35 S00	1.86	400	0		2.5
A35 S10	1.86	360	40		2.5
A40 P06	1.86	376		24	2.50
A40 P08	1.86	368	3.92 [b]	32	2.50
A35 P06	1.86	376		24	2.5
A40 C02	1.86	392	8 [a]		2.50
A40 C03	1.86	388	12 [a]		2.50
A35 C02	1.86	392	8 [a]		2.5
OPC1	0.87			387.9	
OPC2	1.86			428.3	

[a] CH, calcium hydroxide. [b] Superplasticizer.

From the evaluation of the result, the condition for Na_2SiO_3/NaOH of 2.5 satisfies the optimum compressive strength for concrete using an alkaline solution. It appears that a further increase in GGBS would match with the control mix OPC2 since an addition of 20 kg/m^3 of GGBS to A40 S10 results in a maximum strength of 43.2 MPa. The impact of calcium hydroxide to attain the optimum strength is minimal compared to GGBS. It is obvious from the results that the use of an alkaline solution and GGBS significantly impact the compressive strength of concrete, and the use of additional water for concrete with an alkaline solution is, adversely, not necessary, as it tends to neutralize the hydration process. A comparative study of the different concrete mix constituent materials according to [33],

and as presented in Table 5 shows that a high mechanical response for 45% of cement and 55% fly ash resulted to a compressive strength of 40 MPa and a flexural strength of 12.8 MPa respectively.

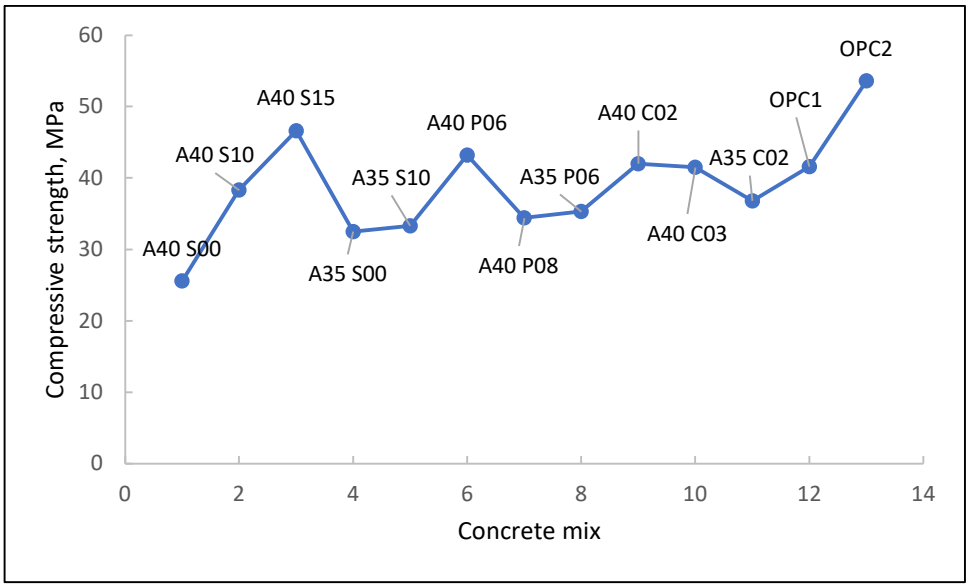

Figure 2. Compressive strength of geopolymer concrete.

To study the effect of silica fume and GGBS on recycled aggregate concrete (RAC), Mouna, Batikha and Suryanto [34] carried out an experimental program using some locally manufactured recycled aggregate. The results indicate a reduction in the mechanical performance in comparison with the control mix owing to the porosity of the recycled aggregate (RCA) due to a pre-existing history of cracks during the crushing process. The contact zone structure in concrete that exists between cement and aggregate is responsible for the formation of a collapse mechanism when it is placed under load. Destruction in normal concrete takes place in the contact zone, i.e., the cement matrix/aggregate is known as the weakest link in the structure of the concrete, as the LWC does not follow the three-stage crack development (I—formation of stable features, II—stable crack propagation, III—unstable crack propagation) that is common in normal concrete. In normal concrete, stage I propagates into II at compressive stresses amounting to 30–40% of concrete strength, usually within the elastic zone, while stage II moves to stage III at stresses of about 70–90% of strength.

The cementitious activity of a material is determined by its chemical composition and material fineness, which eventually affect its reactivity. Tables 6 and 7 show that silica fume does not contain sufficient cementitious materials compared to GGBS; however, it possesses high pozzolanic activities. Regarding their reactivity, the fineness of a material contributes immensely to its reactivity. GGBS has a fineness of about 450 m^2/kg compared to Portland cement of 350 m^2/kg, but that of silica fume is 15,000–30,000 m^2/kg. The mechanical properties of concrete can be enhanced using silica fume, which has a high specific area that is sufficient in reducing the carbonation and enhancing good hydration when used in combination with a binder.

2.3. Flexural Strength

A fundamental measure of concrete performance is based on the assessment of certain parameters that significantly affect the behaviour of the concrete. One such parameter is the flexural strength of the concrete, which is a measure of the flexural resistance to bending. A requirement for structural lightweight aggregates conforming to the requirements of ASTM C 330 set the tensile splitting strength of 290 psi (2.0 MPa) as the minimum for lightweight

concrete, while the flexural strength is about 10 to 15 percent of the compressive strength with consideration of the concrete mixture using ASTM C78 [40].

Table 6. Typical ranges of chemical compositions for the major oxides present in UK cementitious materials [35].

	CEM1 %	GGBS %	Silica Fume %
CaO	60–70	35–45	<1
SiO_2	20–22	33–40	35–50
Al_2O_3	4–7	8–16	<1
MgO	1–3	7–15	<4

Table 7. Chemical and physical properties of binders [36–39].

Property	Portland Cement	Siliceous Fly Ash	GGBS	Silica Fume
SiO_2	21.9	52	35	85–97
Al_2O_3	6.9	23	12	
Fe_2O_3	3	11	1	
CaO	63	5	40	<1
MgO	2.5			
SO_3	1.7			
Specific surface (m^2/kg)	370	420		15,000–30,000
Specific gravity	3.15	2.38	2.94	2.22

2.4. Flexural Strength

A fundamental measure of concrete performance is based on the assessment of certain parameters that significantly affect the behaviour of the concrete. One such parameter is the flexural strength of the concrete, which is a measure of the flexural resistance to bending. A requirement for structural lightweight aggregates conforming to the requirements of ASTM C 330 set the tensile splitting strength of 290 psi (2.0 MPa) as the minimum for lightweight concrete, while the flexural strength is about 10 to 15 percent of the compressive strength with consideration of the concrete mixture using ASTM C78 [40].

Well-compacted concrete specimens with mineral admixtures (such as silica fume and fly ash) with a high binder content are not permeable and will release water very slowly. This is observed from the physical examination of splitting tensile test specimens containing dry specimens, which will cause defects in flexure from crack propagation. The use of FA at high volume in concrete helps in improving the mechanical properties of the concrete by lowering drying shrinkage with a good influence on workability and durability. It is also observed that the problem of alkali reaction in concrete which leads to concrete poor performance is reduced with the use of FA, but there is a delay in the hydration process, which causes a reduction of strength at an early age [41]. Similarly, it was observed from the study by [34] that the use of silica fume in concrete causes a reaction with calcium hydroxide, which is very active in the cement hydration process. This is used to improve the mechanical behaviour of concrete, which leads to early strength formation. Regarding the use of SCM, there have been reports of cases of low deformation capacity and crack formation associated with low-carbon concrete under service loads. Improvement of poor deformation is reduced using a blend of glass fibre to enhance the cracking and tensile strength of the composite low-carbon concrete and the aggregate should be classified in conformity to requirement of BS EN 13055 [42].

To increase the fracture toughness of LWC arising from increasing the crack propagation and from reducing the defects in flexural resistance, the use of fibres and nano materials is beneficial on the ductility of the concrete specimen. The improvement of the mechanical properties of the concrete with the use of geopolymer materials and carbon nanomaterials, such as carbon nanotubes (CNTs), carbon nanofibres (CNFs), and graphite

nanoplatelets (GNPs) as investigated by [43], is proven to be effective in concrete strength improvement. The use of fibre in the mix for LWC with the mono-plastic fibres shows significant increases in flexural strength compared to NWC. A study conducted on the use of fibre shows that flexure strength increases by 19.5%, 37%, 33.9% and 34.2% at 7, 28, 60, 90 days, respectively, compared to NWC. The addition of fibre in the LWC was shown to have arrested the propagation of cracks; however, a decrease in the modulus of elasticity was recorded by about 11.7% and 5.1% at 28 and 90 days, respectively, compared with NWC [44]. The prediction of crack control by a multi-phase model using pumice as the LWA and reinforced with hooked steel fibre increases the flexural strength of the concrete specimen [45]. The use of fibre on recycled aggregate concrete sometimes decreases workability, but improvement in mechanical properties was achieved with the crack bridging action of steel fibres [46]. Expanded shale aggregates were sintered in an experimental work in comparison to steel fibre. On continuous application of the load, it was shown that the toughness of the fibre increases significantly at peak load [47]. The use of lightweight clay aggregates with hooked steel fibres between 0 and 1.15% was used to increase the fracture energy of LWC. When the Steel fibre content was increased from 10 to 90 kg/m^3 (0.13–1.15 vol%), the characteristic length increased 3.6, 4.4, 5.0, 7.5, and 11.0 times in comparison with the fibre-free specimens. Similarly, concrete mixes with steel fibre contents of 20–90 kg/m^3 (0.26–1.15 vol%) increased by 1.4, 1.5, 1.6, 2.1 times for the SF10 samples, and an increase in ductility was reported [48].

Evaluation of the tensile strength of LWC that undergoes drying shows a correlation with the shear strength of the concrete structure. The moisture loss during drying increases at a slow rate into the concrete, which brings about the development of tensile stresses at the exterior faces that invariably balances the compressive stresses developed. The flexural resistance is often represented as the fracture energy formed per unit area of crack developed.

The mechanical properties of recycled aggregate concrete were studied by Chinzorigt et al. [49] to investigate concrete strength development using 30% to 100% aggregate replacement. It was observed as shown in Figure 3 that the compressive strength reduces with an increase in RCA replacement, while specific creep of the specimen with 100% RCA increased by 38% when compared to the normal concrete.

In lightweight aggregate concrete, the first load-induced cracking appears and propagates directly at stresses of 85–90% of the compressive strength [50].

For normal concrete, the stress–strain curve at the elastic region occurs at about 45% of the ultimate compressive strength of the concrete, which is indicative of relatively low elastic energy stored in the system. From analysis, an ideal stress–strain relation for concrete exhibits a nonlinear relation, as the strain due to an applied load is nonrecoverable. However, for a sintered aggregate such as RCA, studies by Zhang and GjØrv [51] have shown that the straight line in the stress–strain curve within the elastic region extends up to 90% of the compressive strength, which implies a high elastic energy stored in the concrete that is responsible for the rapid crack propagation and collapse of the concrete.

Regarding the use of GGBS and silica fume as a combined binder in a concrete mix, the result from the study conducted by Mouna, Batikha and Suryanto [34] and result shown in Figure 4 indicates that the compressive strength at 50% replacement of cement with GGBS and 10% replacement for silica fume show a reduction in strength in comparison to other mixes. One influencing factor for the low strength of M3, as shown in Figure 4, is the density of 2294 kg/m^3, while M1 with the highest strength with a density of 2480 kg/m^3, attained a remarkable compressive strength of 67 MPa. The water-to-cement ratio of 0.3 for M3 was not enough for the complete hydration reaction of GGBS and silica fume composition. This means that to attain higher strength for RAC, a low water-to-cement (w/c) is required, while the same value of w/c is not enough for the complete hydration of the GGBS and silica fume combination in the mix to attain same strength. The behaviour of GGBS and silica fume can be likened to its physical and chemical composition.

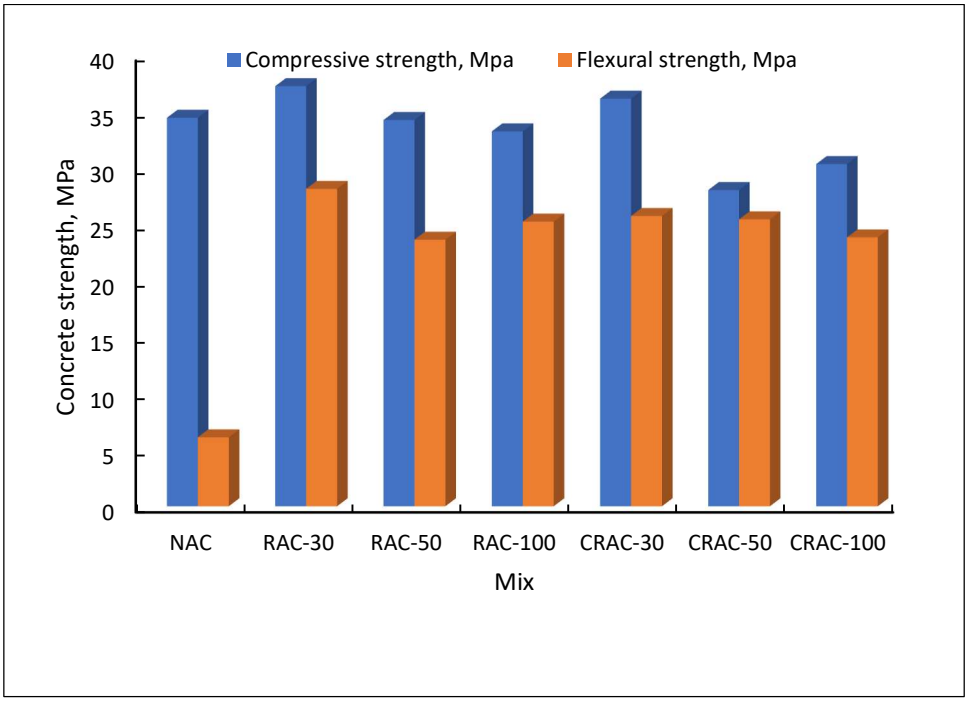

Figure 3. Strength comparison of concrete mix. NAC, natural coarse aggregate concrete; RAC-30, recycled aggregate concrete at 30% replacement; RAC-50, recycled aggregate concrete at 50% replacement; RAC-100, recycled aggregate concrete at 100% replacement; CRAC-30, carbonated recycled aggregate at 30% replacement; CRAC-50, carbonated recycled aggregate at 50% replacement; CRAC-100, carbonated recycled aggregate at 100% replacement.

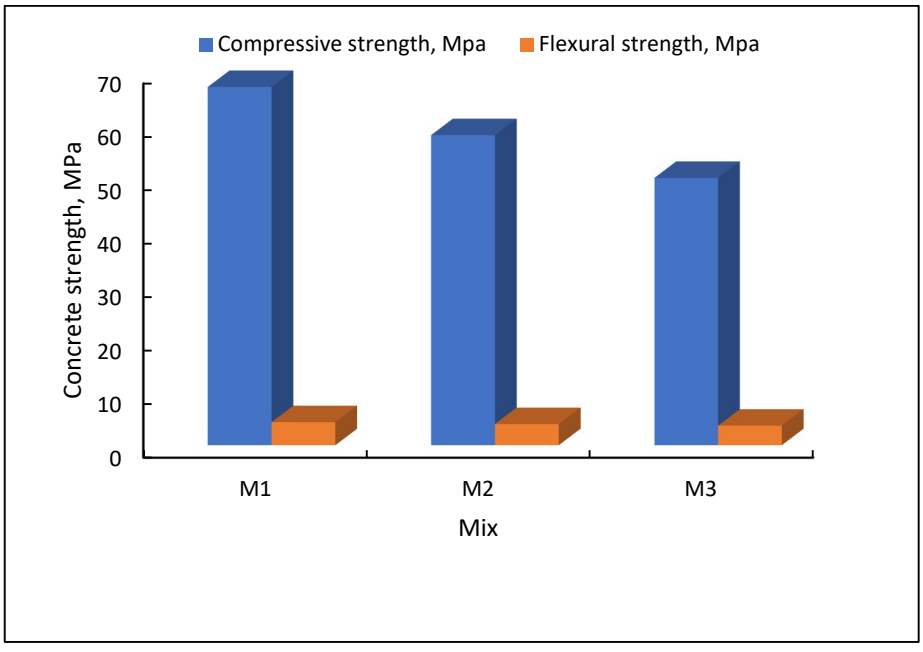

Figure 4. Strength comparison of concrete mix. M1 = control = 100%OPC + 0% RCA +0% GGBS + 0%SF. M2 = 100%OPC + 100%RCA + 0%GGBS + 0%SF. M3 = 40%OPC + 100%RCA + 50%GGBS + 10%SF.

An experimental program was conducted using sintered fly ash (artificial aggregate known as Certyd) as a LWA on two concrete mixes of different compositions at densities of 1810 and 1820 kg/m^3 for LC50/55 according to Eurocode 2 [27] for light-weight concrete by Szydłowski and Łabuzek [52]. The result obtained shows a very low creep and shrinkage

with a high compressive and flexural strength, as shown in Figure 5. The control used is water, with a difference in the two mixtures, mainly the water content and the W/C ratio. The C-1 mixture consists of 164 L of water per cubic meter, and C-2 consists of 209 L according to [52] and as shown in Figure 5. The water content and W/C ratio (0.41 and 0.51) show an average compressive strength after 28 days at 56.9 MPa for C-1 and at 58.4 MPa for C-2. This is an indication that for LWC, enough water is needed for full hydration.

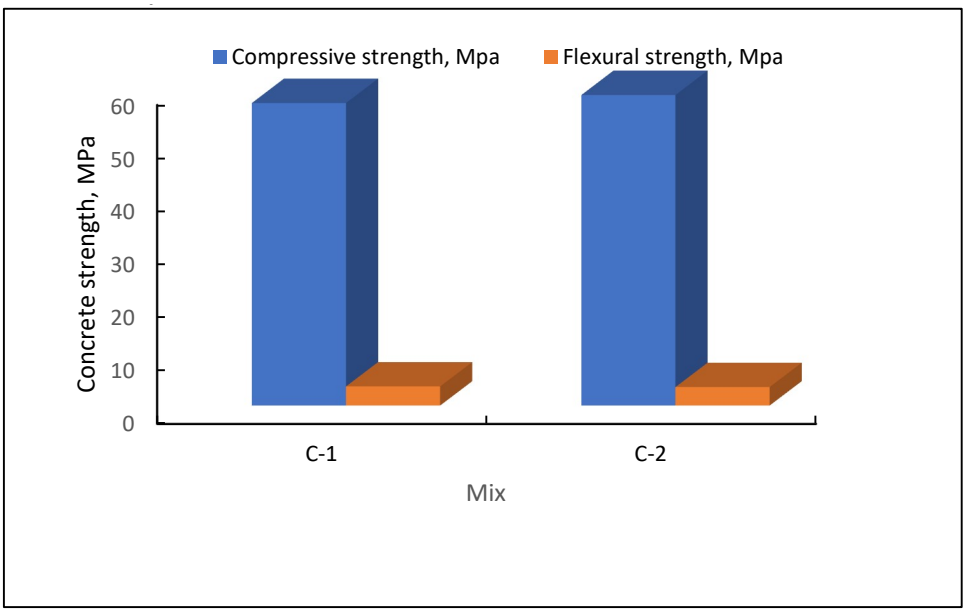

Figure 5. Strength comparison of concrete mix.

From Table 8, the use of different kinds of fibres and their effects on mechanical properties such as compressive strength, flexural strength, toughness, and bending are significant on light-weight concrete. The use of fibre in concrete reduces the extent of crack propagation as well as improves the flexural properties [53–55]. Polypropylene shows a maximum elongation compared to carbon and steel fibre, which makes its suitable for flexure. This implies that when compressive strength is desirable, the use of steel fibre will be appropriate considering the density of 7.8 g/cm^2; polypropylene will be appropriate for tension or flexural strength resistance.

Table 8. Properties of three types of fibre [55].

Properties	CF *	SF **	PF ***
Length (mm)	5	25	15
Diameter (mm)	7	500	100
Density (g/cm^2)	1.6	7.8	0.9
Modules (GPa)	240	200	8
Elongation at break (%)	1.4	3.2	8.1
Tensile strength (MPa)	2500	1500	800

* Carbon fibre, ** Steel fibre, *** Polypropolene fibre.

Fly ash is a product of industrial waste from coal-firing power stations, which contains mainly ferric oxide (Fe_2O_3), aluminium oxide (Al_2O_3), silicon dioxide (SiO_2), and calcium oxide (CaO), as shown in Table 9. It has been shown to contribute to reducing embodied carbon in concrete when used as a SCM material. It can form a denser concrete matrix, which makes it a good pozzolan due to the presence of SiO_2 and Al_2O_3; however, the result from [54] shows a decrease in flexural strength observed with an increase in fly ash.

Table 9. Review of mechanical responses of low-carbon concrete.

Reference	Concrete Mix (%)	Compressive Strength (MPa)	Flexural Strength (MPa)
[56]	CM30-PFA40-SF5-LS15	37	
	CM30-PFA40-SF5-LS25	34	
	CM30-PFA60-SF5-LS5	30	
Zhu et al. [57]	CM20-PFA80	40	4.3
Şahmaran et al. [58]	CM31-PFA69	39	7.8
	CM20-PFA80	37	8.6
[59]	CM45-PFA55	40	9.1
Siad et al. [60]	CM28-PFA62-LS10	38	8.2
	CM28-PFA55-LS20	36	8.1
Halvaei et al. [61]	CM45-PFA55	40	12.8
[62]	CM20-PFA65-PI5	36	

CM, Portland cement; PFA, Pulverised Fly ash; LS, limestone; SF, silica fume.

A mix design developed by Alma'aitah and Ghaissi [56] using a range of ternary and quaternary blended concrete mix using fly ash, limestone, silica fume and ordinary Portland cement at 70% to 80% cement replacements resulted in 31% and 25% carbon footprint and embodied energy, respectively. This is in comparison to the control mix of 45% Port land cement and 55% fly ash, where an increase in limestone from 5% to 15% shows compressive strength increase from 30 to 37 MPa but with a decrease to 34 MPa in LS of 25%. This can be explained from the mechanical composition of their constituent materials, as shown in Table 9 for which the microstructural merits over the concrete mix consist of the formation of an amorphous alumino-silicate gel, which is reported to have good mechanical properties. The inclusion of fly ash with 82.55% of SiO_2, AL_2O and Fe_2O_3 introduces the formation of more calcium silicate hydrate gel (CSH), which modifies the flexural capacity of the concrete. An increase in flexural strength depends mostly on the cement-to-fly-ash ratio rather than percentage addition of [55]. From the analysis of Tables 9 and 10, when the concrete composition is PC45FA55, the cement-to-fly-ash ratio is 0.81, with a flexural strength of 12.5 MPa. However, for Zhu et al. [57], with a cement-to-fly-ash ratio of 0.25, the percentage of fly ash is 80%, and the flexural strength is 4.3 MPa.

Table 10. Chemical composition of PC, FA, SF and LS [35].

Chemical Composition %		CM	PFA	SF
CL-	%	0.05	0.01	0.3
SO_3	%	3.34	0.65	2
CaO	%	64.72	4.63	1
SiO_2, AL_2O, Fe_2O_3	%	27.34	82.55	
Na_2O	%	0.23	2.52	
MgO	%	1.09	1.85	
PO_4	%		0.39	

CM, Portland cement; PFA, Pulverised Fly ash; LS, limestone; SF, silica fume.

The aggregate is generally stronger than the matrix for the normal-weight concrete and cracks typically in the matrix or along the matrix–aggregate interface when concrete is subjected to a tensile stress. Crack propagation may be arrested by aggregate particles, which will be shown in the form of meandering and branching of cracks that may cause a gradual weakening of the concrete. However, for the light-weight concrete, the cracks are propagated through the aggregate due to its light density and may result in a collapse of the concrete.

Concrete collapses are mitigated using fibre reinforcement as this tends to enhance early strength of concrete [63]. A study of reinforced concrete plastic was conducted by [64].

Reinforced steel fibres of weight 35 kg were added to the concrete mix using GGBS at 50% cement replacement to investigate the effect of fibre on the concrete plastic and strength properties. A higher water demand was noted in the mix compared to the control mix, which was attributed to the higher fineness of the GGBS. Higher early aged strength was also observed compared to the control mix, with a 20% increase in flexural strength at 56 days. The effect of drying shrinkage in concrete keeps the applied stress within a tolerable limit to avoid a fall back. There was a significant decline in shrinkage compared to the control with a 50% reduction at 28 days and 43% at 56 days, with about a 20% reduction in embodied carbon. Similar results were observed in the debonded concrete overlays and in the use of SCM materials for soil stabilization [65–68].

2.5. Creep and Shrinkage of LCC

Creep deformation is formed because of the viscoelastic behaviour of concrete when placed under load and commences after the origination of elastic deformation. Creep and shrinkage are phenomena that describe the long-term deformation in concrete to characterize its behaviour under permanent load. Creep is the time-dependent deformation of concrete under a particular load. The increase in length or size of the material under load can affect the serviceability of the structure, as there can be reduction in safety margin against collapse due to long-term growth of the deformation. The accentuation of creep is seen after the application of load with an increase in deformation, but it reduces as the age increases with a tendency to attain stability within one year. The aggregate in a hydrated concrete matrix with cementitious binder initiates propagation of creep [69,70].

When an initial load is applied on a concrete structure, there is an initial modulus of elasticity generated within the concrete, and as the load continues, there will be gradual reduction in the concrete strength as well as in the initial modulus of elasticity. Continuous deformation in concrete is observed in the concrete due to the applied load until the applied stress is equal to a certain value of the concrete characteristic strength, for which stability is attained. The strain obtained at that point of stability is the ultimate creep strain which is found to be greater than the elastic or initial strain. The ratio of the ultimate creep strain to the elastic strain is the creep coefficient ‘φ. This can be expressed as $‘\varphi = \frac{\varepsilon u}{\varepsilon}$, where εu is the ultimate creep strain at time t, and ε is the elastic strain or the initial strain. The final modulus of elasticity is then determined as a function of the creep coefficient that describes the behaviour of the concrete as a long-term deformation effect. The increase in relative humidity (RH) improves the hydration process and consequently results in a decrease in the creep strain and an increase in the compressive strength of the concrete.

It can be expressed as $Efinal = \frac{\text{Einitial}}{1+‘\varphi}$, where *Efinal* is the final modulus of elasticity, and *Einitial* is the initial modulus of elasticity.

The factors that influence the extent of creep strain in the concrete includes water-to-cement ratio, cement-paste-to-aggregate ratio, ambient temperature, and air entrainment (air pocket within concrete). There is likely to be more error in the determination of creep and shrinkage properties of the material than that of a structural analysis. Creep analysis is useful for the prediction of life expectancy before service, modelling the behaviour of the material at constant load with very high temperature, and to model strain-limited long-term applications [71]. The creep behaviour in LWAC is reported to continue at later days compared to the NWC. As the cement content in concrete increases, there is a complimentary increase in creep for the NWC with the same water content and load; however, compressive creep increases with a reduction of cement content. The latter is true, as creep is a function of the content of cement volume for the paste in concrete [72].

The effect of relative humidity on the geopolymer concrete was shown to improve the creep and shrinkage by varying the curing regimen of the specimen at elevated temperatures of 40 °C. The geopolymer binder is made of 85.2% calcium fly ash and only 14.8% GGBFS (ground granulated blast furnace slag). Creep strains at 3 days were reduced to about 70% and were relatively near zero at 80 °C compared to the control mix of the normal-weight concrete [73]. From the oxide composition of GGBS, high-performance

fly ash and fly ash, the geopolymer mixture has higher SiO_2, CaO and Fe_2O_3, which is sufficient to enhance heat of hydration through the production of alumino-silicate gel at a temperature of about 40 °C. The concrete strength development for long-term creep and shrinkage behaviour of recycled aggregate concrete (RAC) was studied using recycled coarse aggregate (RA) to replace natural coarse aggregate (NA) by 30%, 50%, and 100%. It was observed that while the shrinkage of RAC with 50% RA is like that of NAC, RA of 100% increases over that of NAC to 13% after 180 days, and the specific creep of RAC with 100% RA increased by 38% over that of natural aggregate concrete [49]. The creep coefficient of the different mix is shown in Figure 6, which indicates that the creep coefficient for RAC is at 50% replacement, like that of 100% replacement, while CRAC-50 performed similar to that of the control NAC.

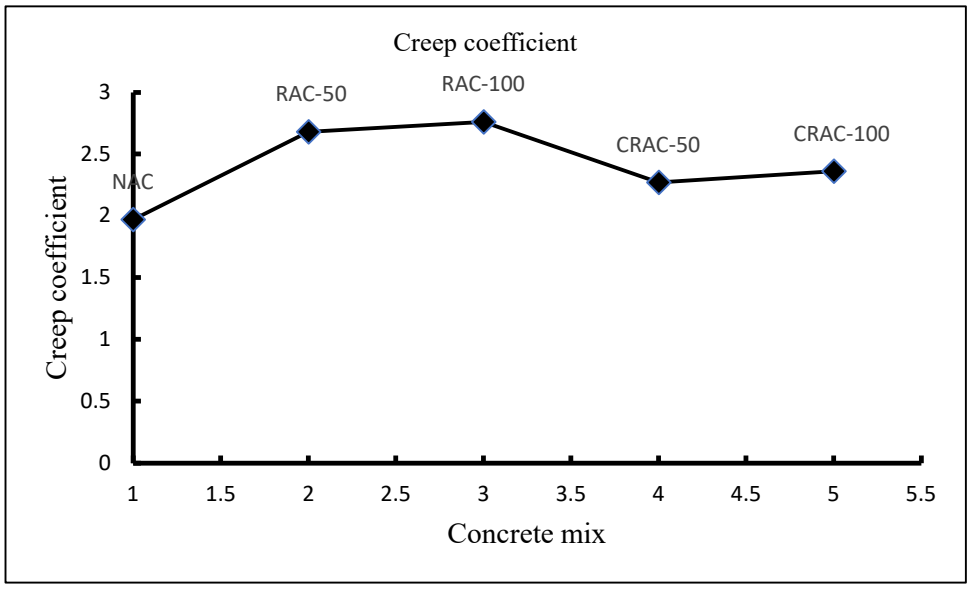

Figure 6. Creep coefficient for RAC.

The material composition of concrete, in terms of the aggregate, contributes to the outcome of creep even in consideration of factors necessary to improve its performance. Replacing secondary aggregate with some clay particles in concrete even for different extreme environment conditions at 100% humidity and air dying shows very low impact for creep. A sample mix for high-strength concrete (HSC) and an admixture of montmorillonite clay mineral nanoparticles (MNP) at about 1% were used in the study. The creep coefficient of the MNP specimen reaches 3.6 and 4.3 for the air dried and moist conditions, respectively, while that of HSC reaches 2.8 to 4.1 for similar specimens [74].

Creep and shrinkage are higher for LWC compared to NWC, which is a consideration in the structural design. Studies has shown that creep for LWC containing lytag increases with an increase in the water-to-cement ratio such that within one year a stress–strength ratio from 0.3 to 0.5 owing to an increase in water-to-cement ratio from 0.54 to 1.02, respectively [75,76]. In assessing the extent of the load-bearing capacity of a concrete structure, creep analysis predicts the limit of failure with an expected strain associated with the loading. This shows that creep increases with the age in loading when using a LWA such as lytag, as shown in Figure 7. Evaluation of the long-term dependent properties and durability of low-carbon concrete was carried by Robalo et al. [77] using fly ash and limestone as a partial replacement up to 70%. The influence of these parameters on the LCC properties such as shrinkage and creep, carbonation, and water absorption by capillarity and by immersion were investigated. The result indicates that concrete compactness is a major dependent variable that improve the long-term deformation of low-carbon concrete.

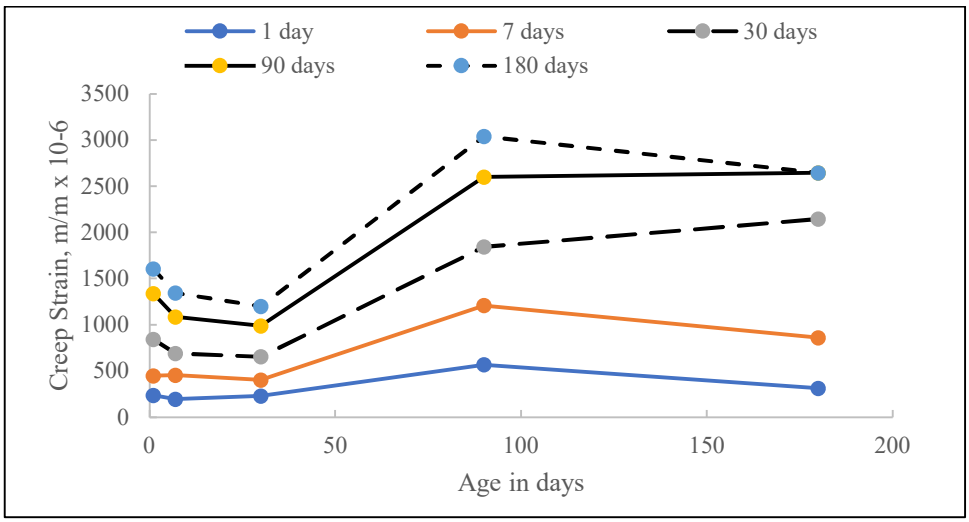

Figure 7. Creep strain associated with age in loading for Lytag concrete.

For the lightweight concrete, creep strain varies between 1 and 1.5 to that of NWC, while test results have shown that the use of higher strength concrete reduces this variation.

Shrinkage is the loss of capillary water from the hardened cement mixture, which usually leads to crack formation and contraction of the concrete. It is usually accompanied with the formation of cracks that weakens the concrete by allowing the passage of harmful agent to the concrete [78].

Drying shrinkage is the change that the concrete volume suffers because of moisture movement changes from ambient temperature or from properties of the material. This arises from the fact that a greater percentage of the water used in concrete does not take part in the hydration process; hence, at the end of concrete curing, there is relatively low relative humidity, for which the gradient between the humidity differential, the surrounding environment, and the concrete propels the movement of the trapped moisture in the concrete to migrate, and the resulting effect is volume change. It is very likely that if the ambient temperature is high, there will be a low gradient accompanied with a low drying rate (low shrinkage). Factors that affect the concrete shrinkage include the water-to-cement ratio, cement content, aggregate concentration and stiffness, and environmental condition, which all significantly contribute to shrinkage in concrete. Studies from [79] show that with increasing aggregate replacement of 100% RCA, there is an increase in shrinkage to about 50%.

From the mix composition of [75], and the analysis of the result presented in Table 11, it can be deduced that concrete strengths of 60 N/mm^2 is obtained using Lytag and sand by using a lower cement content for lightweight concretes to achieve a given compressive strength. The creep coefficients obtained as shown in Figure 8 are comparable with the range of values obtained for concretes made with various dense aggregates. From the concrete mix ratio in Table 11 and with the argument of cement being the major contributor to carbon in concrete, it can be inferred that the mix with the lowest cement content is low-carbon concrete (CR 30-1). A study of the creep coefficient in Figure 8 shows that the LCC (CR30-1) exhibits a high creep in comparison with CR 60-1. This agrees with available literature on creep and shrinkage tests on light-weight aggregate concrete, such that light-weight concrete shows lower creep at higher strength [80–83].

Table 11. Mix composition for lytag sand concrete.

Specimen	28 Day Strength (N/mm^2)	Cement Content (kg/m^3)	Cement: Sand: Lytag Ratio by Weight	Total Water–Cement Ratio
CR 30-1	32	255	1:2.78:2.80	1.02
CR 45-1	44.5	335	1:1.93:2.13	0.78
CR 60-1	58	485	1:1.06:1.47	0.54
CR 30-2	29.5	255	1:2.78:2.80	1.02
CR 45-2	43	335	1:1.93:2.13	0.78
CR 60-2	59	485	1:1.06:1.47	0.54

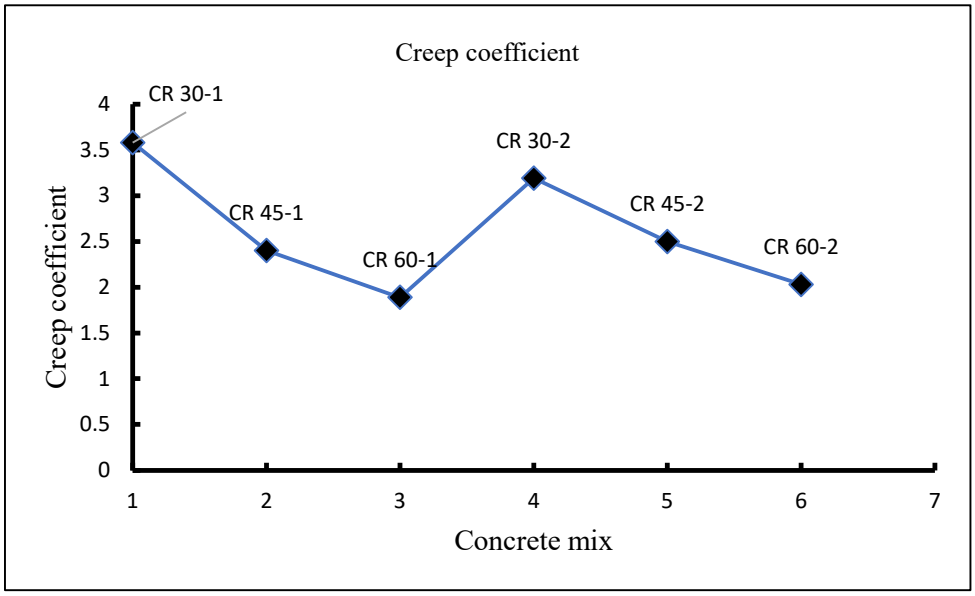

Figure 8. Creep coefficient for lytag sand concrete.

3. Data Analysis Using Artificial Neutral Network (ANN)

The use of ANN requires the availability of a large repository of data to train and fit a data set in such a way that prediction can be visualized to give real-time interpretation. The training algorithm of the ANN used is the Lavenberg–Marquardt (LM) network due to its demand for less time during epoch. Following the extent of correlation that GGBS, silica fume and cement exhibit on compressive strength with their relative frequency shown in Figure 9, it will be necessary to establish a predictive model with any available data and ascertain their impact on the compressive strength.

The variables were fitted to a frequency histogram and are presented in Figure 10 to illustrate the extent of their distribution.

Data Set Modelling

The data set was constructed from data [84–90]. Gandomi et al. [91] recommended a minimum input ratio of three, and for a more reliable model, five. Using a database of 81 for compressive strength, considering three input variables in this work, the database input ratio is 28. From the reviews carried out in this work and input and compressive strength distribution, the influence of the input on compressive strength was established to be influential.

To generate training data, 81 concrete mix data sets were selected based on GGBS, silica fume and cement selected as the input parameters. The data were trained using an artificial neutral network (ANN), and the prediction of the concrete compressive strength indicated good learning of the data set. About 50% of the data set was used as the training set to enable the model to learn from the data set, while 30% was used to validate the prediction.

The validation set was used to optimize the internal structures and the hyper-parameters of the network. The parameters of the network are the weight of the connection between the neurons and the value of the bias. The number of neurons as a hyper-parameter in the hidden layer varied during the training to attain optimal performance. The test set was used to show how well the model can predict an unknown data set at a proportion of 20% of the data set.

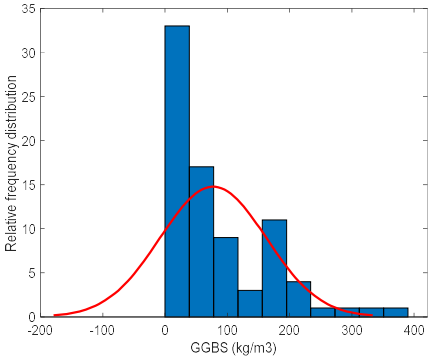

(**a**) GGBS

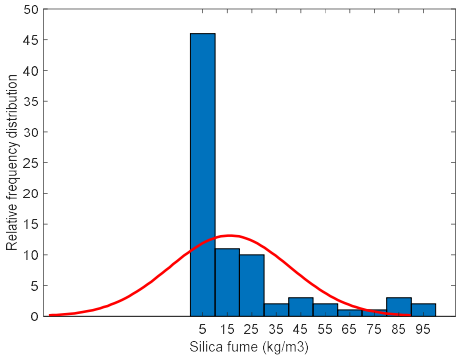

(**b**) Silica fume

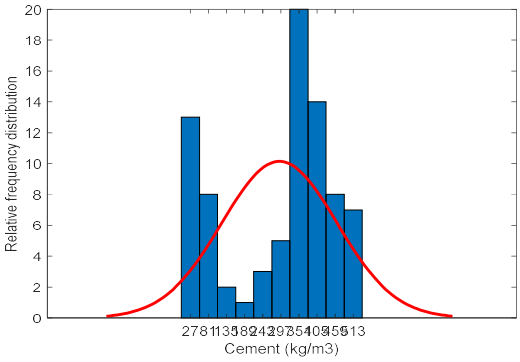

(**c**) Cement

Figure 9. (**a**–**c**) Frequency histogram distribution for input variables.

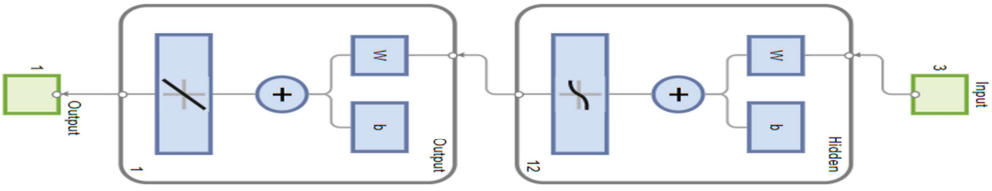

Figure 10. Schematic diagram for the ANN architecture used in analysis, Mathworks Inc. [92].

It is intended to establish whether the complete replacement of cement with GGBS will result in a compressive strength capable of effective structural performance as a novelty of the investigation. The tested data set from the ANN model was utilized as the target output while increasing the GGBS content of the input variables by the total weight of the cement. This implies that the cement attains a 100% replacement with GGBS, and silica fume still maintains its original content. The retrained data set is shown in Table 12.

The training validation and testing of the single layer model using three input variables, twelve neurons in the hidden layer, and one output parameter (ANN model) are shown in Figure 10 The relationships of the input parameters with compressive strength are displayed in Figures 11–14 showing how the direction and magnitude are estimated by computing the derivative of the loss function with respect to the weight while the training stops at a maximum control parameter of 0.1.

Table 12. ANN tested data set for 100% cement replacement.

GGBS, kg/m^3	Silica Fume, kg/m^3	Cement, kg/m^3	Compressive Strength, MPa
100	0	0	30.2494
92.5	7.5	0	64.6554
100	0	0	78.9898
100	0	0	65.6742
95	5	0	56.2174
92.5	7.5	0	62.7031
95	5	0	39.9774
92.5	7.5	0	65.7213
457	0	0	64.1134
457	0	0	72.2078
457	0	0	118.1169
457	0	0	44.4101
535.49	12.27	0	65.7213
518.74	24.54	0	63.1434
501.98	36.8	0	177.5375
529.24	12.27	0	58.2713

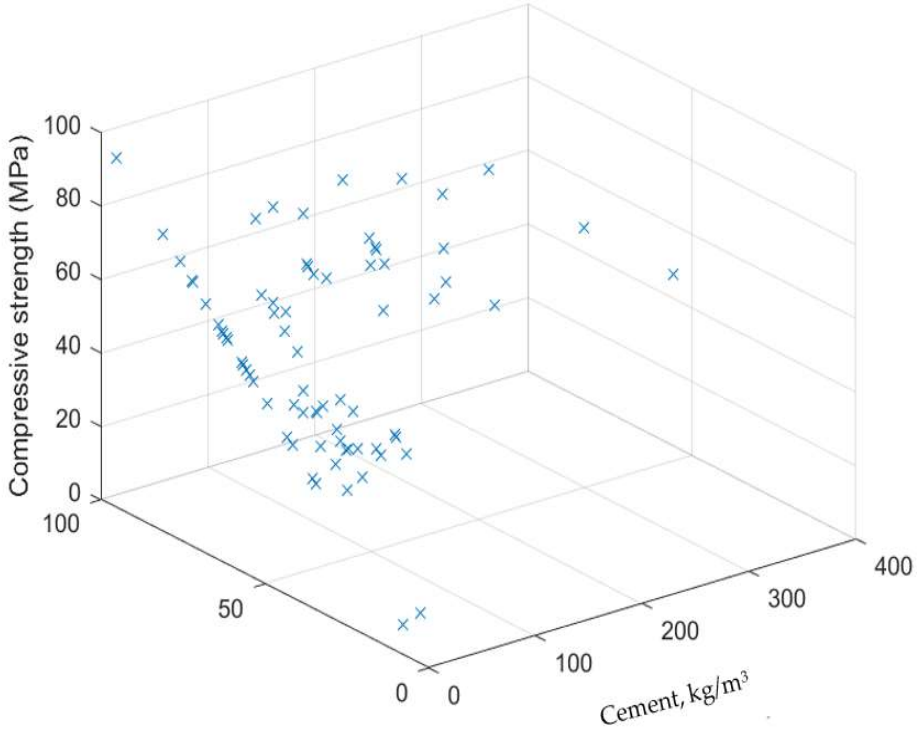

Figure 11. Influence of GGBS on concrete strength.

While GGBS and cement indicate a similar impact on concrete compressive strength, silica fume shows a noisy relationship indicative of a nonlinear relationship with compressive strength. As the epoch increases during the training of the model, there was a decrease in the mean squared error (MSE) resulting in an MSE of 87.64 at the fifth epoch, as shown in Figures 14 and 15. The predicted output from the post training as shown in Table 13 indicates that the regression fits the data points with a correlation coefficient (C) of 0.9184, 0.7910 and 0.8570 for training, validation, and testing, respectively, which is an indication of how well the model performs. This shows that as the epoch increases, the model better learns.

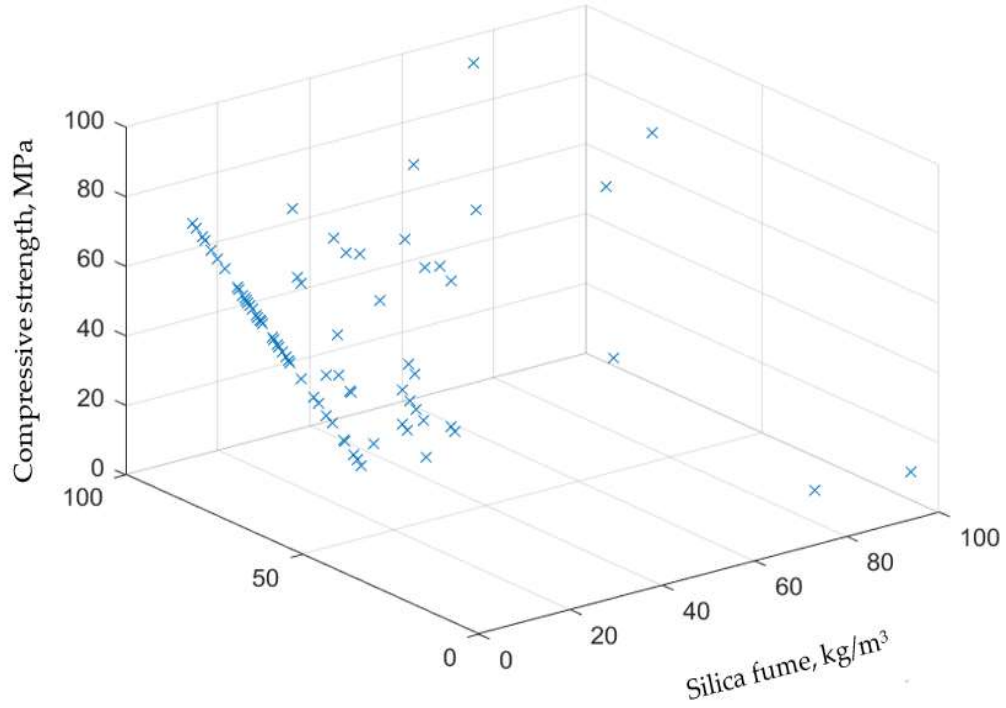

Figure 12. Influence of silica fume on concrete strength.

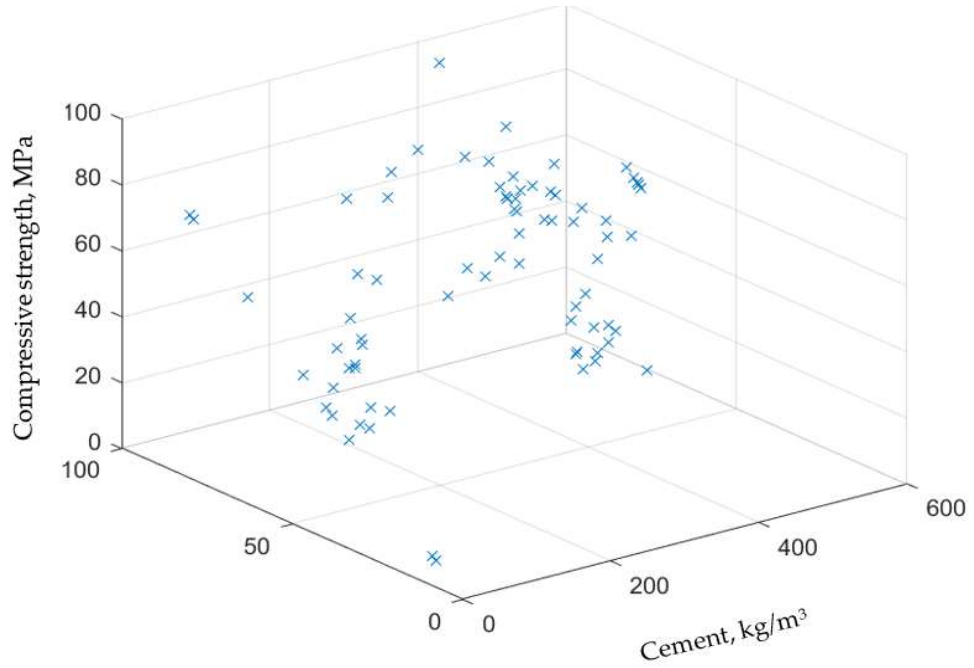

Figure 13. Influence of cement on concrete strength.

The result from the ANN model as represented in Figure 16 clearly shows the effectiveness of the model to learn and predict the compressive strength of concrete using the three variables. The utilization of the tested data at an R^2 value of 0.8495 for the appraisal of the viability of a complete replacement of cement with GGBS portends the roadmap of possibility in concrete decarbonization. Using Figure 17, an optimum number of neurons was selected which enhances the model performance.

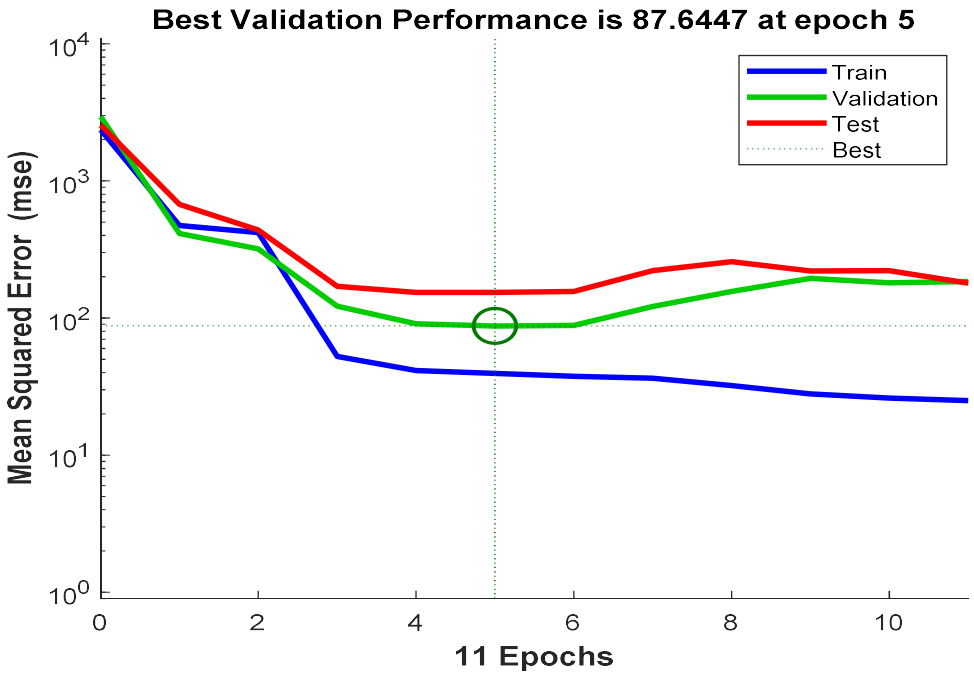

Figure 14. Training and learning profile of single-layer ANN Model.

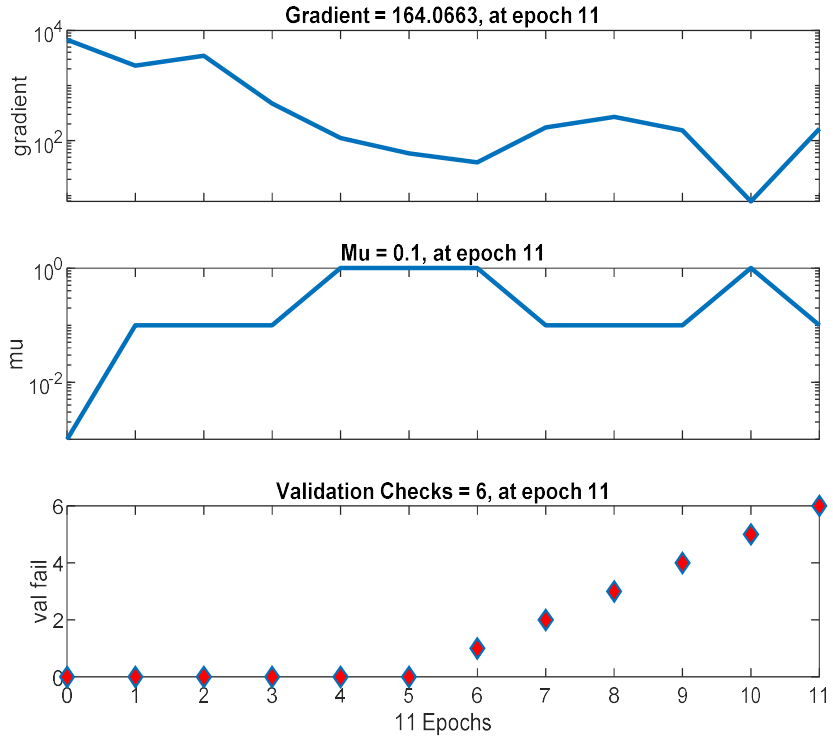

Figure 15. Training and learning profile of single-layer model ANN (3-12-1).

Table 13. Coefficient of determination values (R-squared values, R^2) ANN Network.

Coefficient of Determination R^2			
Training	Validation	Test	Overall
0.9184	0.7910	0.8490	0.8570

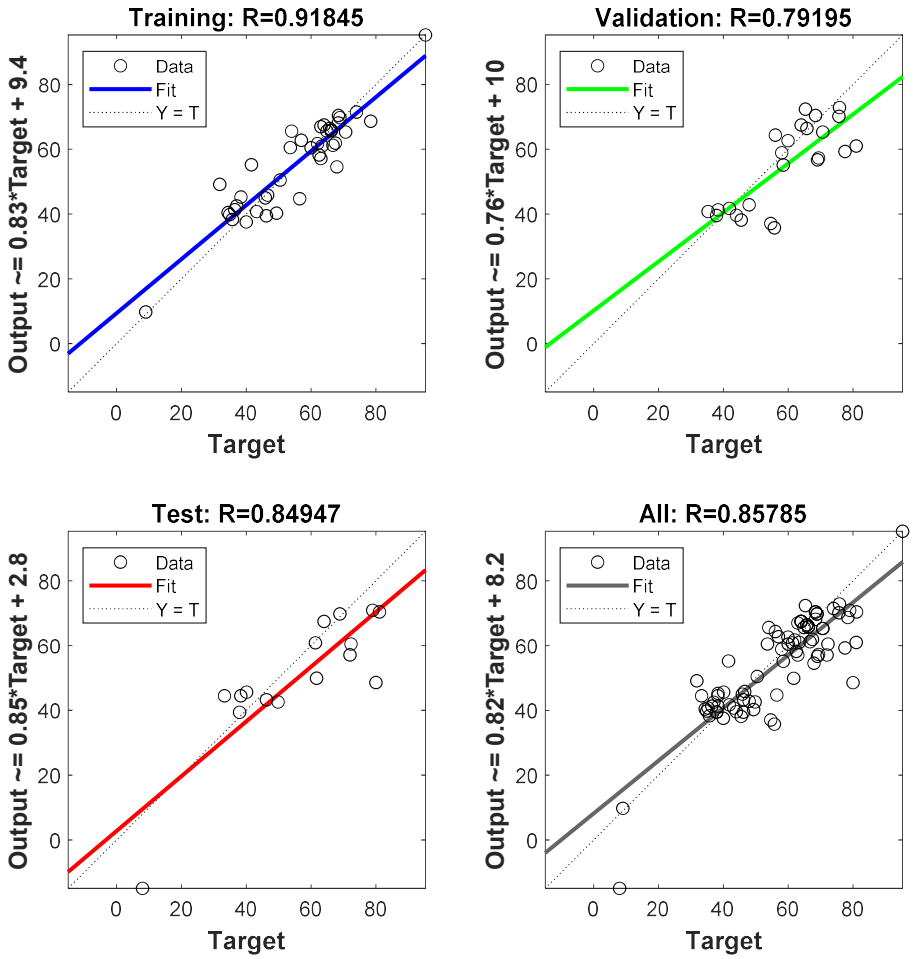

Figure 16. Post-training regression analysis of ANN (3-7-1).

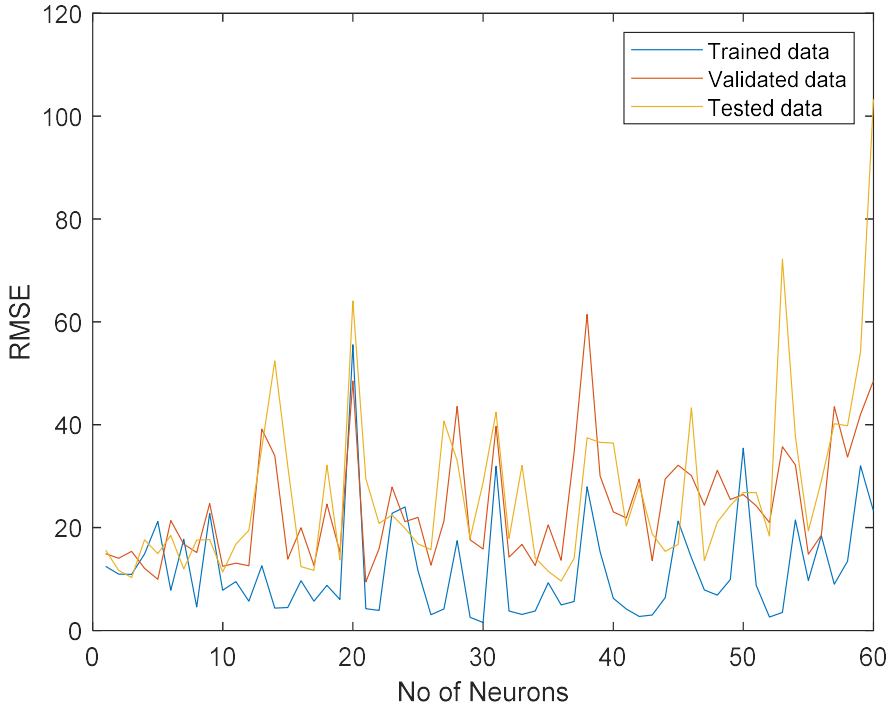

Figure 17. Optimization of neuron in the hidden layer.

4. Complete Replacement of Cement with GGBS

Following the complete replacement of cement with GGBS using the tested data set, a new regimen of training was initiated. There was a reduction in the data sample due to the percentage composition of the tested data sample from the first training at 20% of the data set. The performance at 100% cement replacement is displayed in Figures 18–20, which occur at a best performance of 130.39 MSE for 21 epochs. The mean squared error (MSE) represents the average of the squared differences between the predicted output and the true output. This was used to ascertain whether the prediction was too high or too low to show the correctness of the prediction.

$$\mathrm{MSE}\ (y_{\mathrm{true}}, y_{\mathrm{pred}}) = \frac{1}{n\ sample} \Sigma \left(y_{true} - y_{predicted} \right)$$

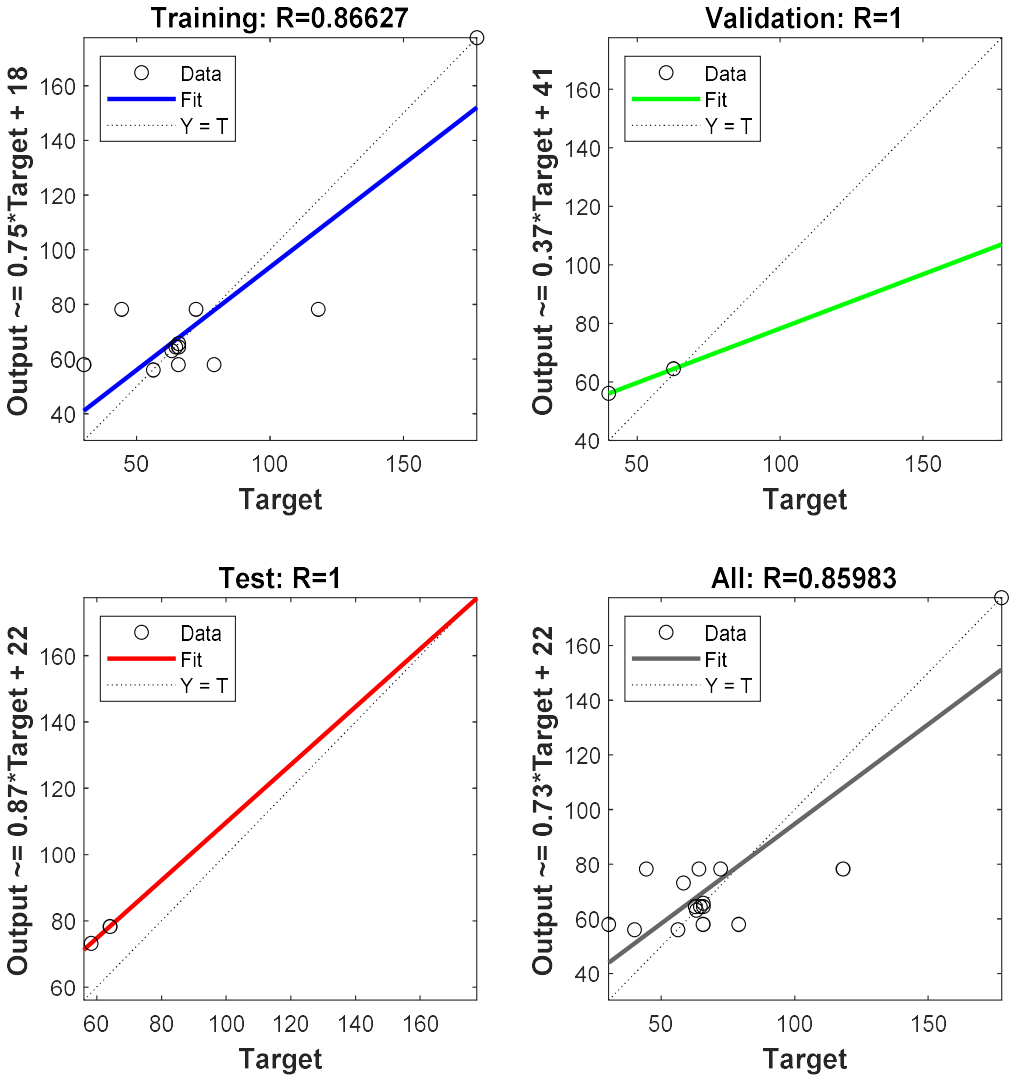

Figure 18. Post-training regression analysis of ANN Model.

The results obtained show that the complete replacement of cement with GGBS is a possibility that will enhance the design and construction of a sustainable concrete using GGBS and silica fume with an overall R^2 of 0.85.

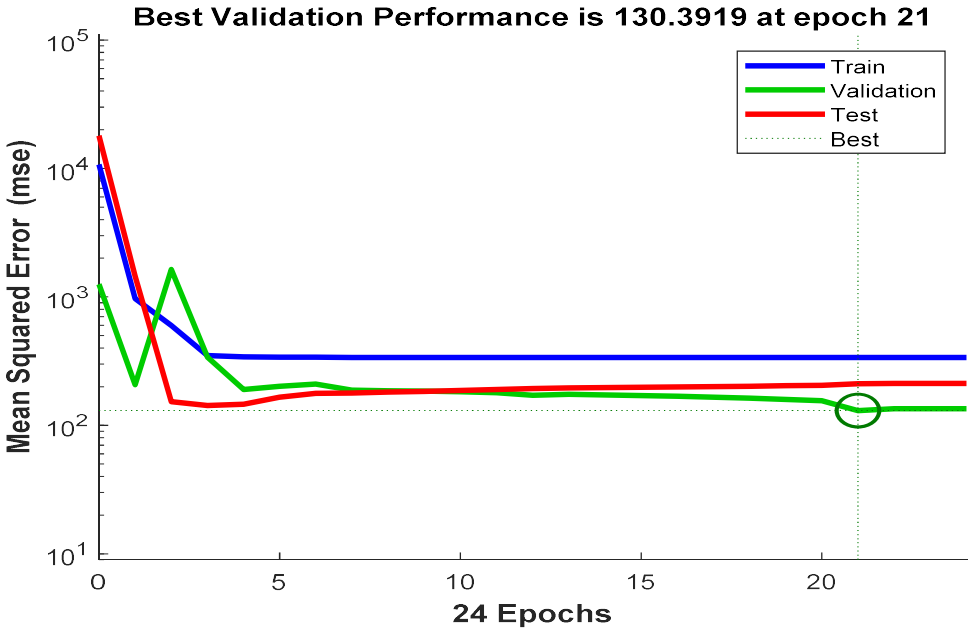

Figure 19. Post-training regression analysis of ANN model.

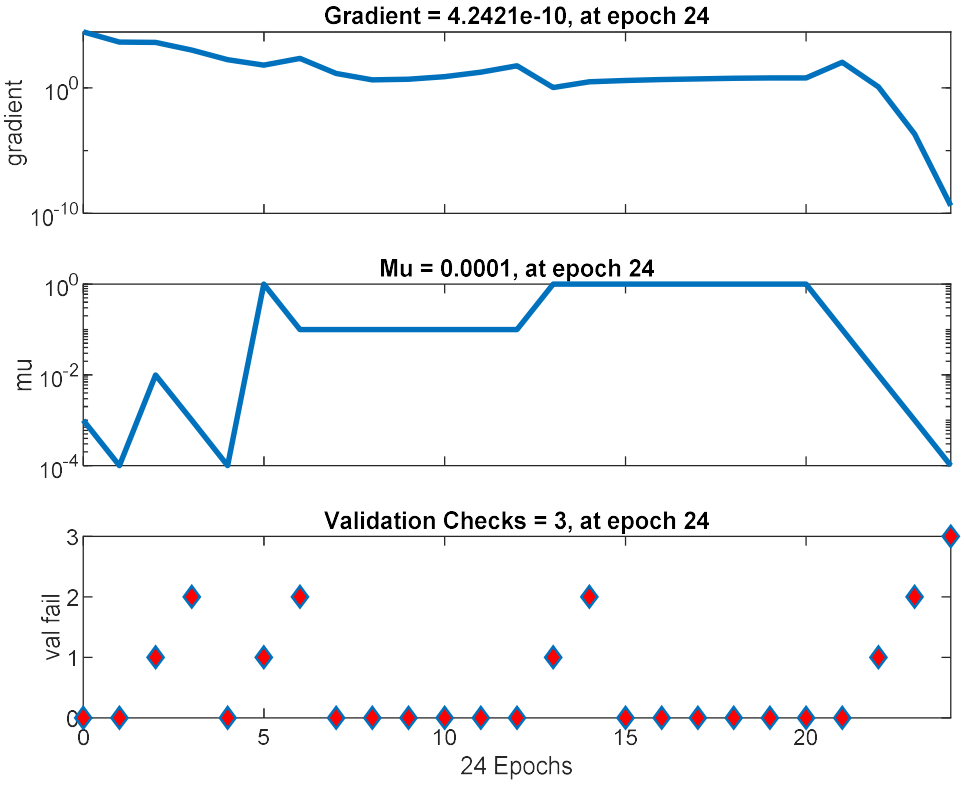

Figure 20. Post-training regression analysis of ANN model.

5. Results and Discussion

The application of three scenarios was evaluated regarding their impact on the mechanical characteries of low-carbon concrete using compressive strength, flexural strength, creep, and shrinkage. The first scenario evaluated is the structural section optimization for the ground beam. It was observed that there is a negligible impact of creep at a coefficient of 0.019 after 365 days on the ground beam if a rectangular section of uniform cross-sectional area is changed to a trapezoidal section while maintaining the total depth of the section.

While the reduction in concrete volume enhances a reduction in embodied carbon, the new section presents an ideal path for effective stress distribution to the soil. There is a remarkable increase in water absorption for the LWC compared to the NWC. This can be attributed to a variation in pores in both concretes, evident by the extent of the depth of carbonation formed. For some concrete with a high depth of carbonation, the formation of calcium hydroxide (CaOH) due to the first hydration is likely to undergo leaching along the path of voids in the paste which will decrease and limit the binder water demand. This can be observed in the form of bleeding during casting and can be quenched with the use of a superplasticizer. However, for the LWC, since cement is often replaced with SCM materials of finer particles of a higher specific surface area, the potential for the formation of the high depth of carbonation is low; hence, an increase in water absorption due to low leaching of CaOH will eventually demand more water for effective hydration. This further shows that the depth of carbonation is dependent on the specific surface area of the binder. Silica fume as a nano material with a specific surface area of 15,000-30,000 kg/m^2 shows evidence of the influence of high specific surface area of concrete binder to enhance its mechanical properties compared to cement of specific surface area of 370 kg/m^2

It is evident from the analysis that LWC of low cement content using lytag suffers a high creep compared to others of high cement content. The density of LWC reduces with time due to the high-water absorption of light-weight aggregate, which is likened to its porosity. This reduction in density continues until an equilibrium density is attained with the ambient temperature; hence, the design of a lightweight aggregate concrete is based on the use of oven-dried density. It is recommended by [76] that lytag requires pre-soaking for 24 hrs prior to mixing to improve the water demand of the aggregate and to eventually reduce creep and shrinkage. The mechanical property of a concrete structure is influenced by load, geometry, material properties and the ratio of the mixed constituent materials. For low-carbon concrete, the reduction in the self-weight on the structure is attained by the choice of a light-weight aggregate concrete and the use of sustainable SCM. The performance of lytag outweighed most light-weight aggregates that were considered. However, analysis of the stress–strain relation for lytag sand concrete indicates that maximum stress was not developed until 30% of the strain was attained, contrary to the normal concrete, where 20% of the strain attained maximum stress. It was also observed that the deformation of the lytag concrete was 1.0 to 1.5 times the deformation of the normal concrete at about 500 days [93]. Using ANN to simulate the possibility of complete replacement of cement with GGBS shows a significant result with an overall fitting R^2 of 0.856. This implies a 10% chance of failure for which inclusion of the concrete additive such as silica fume can mitigate. It was further shown that while the creep coefficient determines the long-term concrete strength, the LCC shows a reduction in creep coefficient for concrete with a high compactness of about 0.9 requires a maximum cement dosage of 175 kg/m$^{3.}$.

6. Future Direction and Limitation of the Study

It is clear from the study that there are uncertainties regarding other influences on the mechanical properties of LCC with the variation of certain concrete parameters. A large data set of low-carbon concrete constituents was scarce and limited for training in ANN, hence the use of 81 available data sets used in the prediction analysis. It is necessary to further investigate the following, as they are not covered in this study:

1. The effect of alkaline solution in low-carbon concrete on the formation of depth of carbonation.
2. Improvement in the mechanical properties of low-carbon concrete due to the age of pre-soaking of lightweight aggregate.
3. The effect of water in a geopolymer concrete using light-weight aggregate.

7. Conclusions

From the results of the study, the following conclusions can be reached:

1. The flexural strength of a low-carbon concrete increases as the cement to SCM ratio reaches 0.8.
2. In optimizing SCM in LCC, the specific surface of the alternative should be considered as a dependent parameter.
3. For concrete stress less than one-third of the characteristic strength, the ultimate creep strain is found to be proportional to the elastic strain.
4. Embodied carbon in the ground beam can be reduced using the trapezoidal section as a conservative cross-sectional area without compromising the structural integrity of the structure.
5. The complete replacement of cement with GGBS shows a good result with an MSE of 0.856.
6. A sodium silicate to sodium hydroxide ratio of 2.5 is optimal to attain a good alkaline solution in a concrete mix.
7. The complete replacement of cement with GGBS is possible when used in combination with silica fume without compromising the compressive strength of the concrete.

Author Contributions: Conceptualization, P.D.N.; methodology, P.D.N.; software, P.D.N.; validation, P.D.N., S.J.A. and C.A.B.; formal analysis, C.A.B.; investigation, J.O.; resources, S.J.A.; data curation, J.O.; writing—original draft preparation, P.D.N.; writing—review and editing, S.J.A.; visualization, S.J.A.; supervision, J.O.; project administration, C.A.B. All authors have read and agreed to the published version of the manuscript.

Funding: University of the West of England, Bristol Funded PhD Studentship.

Institutional Review Board Statement: Not applicable.

Informed Consent Statement: Not applicable.

Data Availability Statement: Not applicable.

Conflicts of Interest: The authors declare no conflict of interest.

References

1. Thacker, S.; Adshead, D.; Fay, M.; Hallegatte, S.; Harvey, M.; Meller, H.; O'Regan, N.; Rozenberg, J.; Watkins, G.; Hall, J.W. Infrastructure for sustainable development. *Nat. Sustain.* **2019**, *2*, 324–331. [CrossRef]
2. Institution of Structural Engineers. Great Britain, British Cement Association and Concrete Centre (Great Britain). In *Manual for the Design of Concrete Building Structures to Eurocode 2*; Institution of Structural Engineers: London, UK, 2019.
3. Müller, H.S.; Haist, M.; Vogel, M. Assessment of the sustainability potential of concrete and concrete structures considering their environmental impact, performance and lifetime. *Constr. Build. Mater.* **2014**, *67*, 321–337. [CrossRef]
4. Habert, G.; Roussel, N. Study of two concrete mix-design strategies to reach carbon mitigation objectives. *Cem. Concr. Compos.* **2009**, *31*, 397–402. [CrossRef]
5. World Business Council for Sustainable Development. The Business Case for Sustainable Development: Making a Difference towards the Earth Summit 2002 and Beyond. *Corp. Environ. Strategy* **2002**, *9*, 226–235. [CrossRef]
6. Quillin, K. Performance of belite–sulfoaluminate cements. *Cem. Concr. Res.* **2001**, *31*, 1341–1349. [CrossRef]
7. Sizirici, B.; Fseha, Y.; Cho, C.-S.; Yildiz, I.; Byon, Y.-J. A Review of Carbon Footprint Reduction in Construction Industry, from Design to Operation. *Materials* **2021**, *14*, 6094. [CrossRef]
8. Haque, M.; Al-Khaiat, H.; Kayali, O. Strength and durability of lightweight concrete. *Cem. Concr. Compos.* **2004**, *26*, 307–314. [CrossRef]
9. Wang, R.; Hu, Z.; Li, Y.; Wang, K.; Zhang, H. Review on the deterioration and approaches to enhance the durability of concrete in the freeze–thaw environment. *Constr. Build. Mater.* **2022**, *321*, 126371. [CrossRef]
10. Perfilov, V.; Oreshkin, D.; Zemlyanushnov, D. Concrete Strength and Crack Resistance Control. *Procedia Eng.* **2016**, *150*, 1474–1478. [CrossRef]
11. Ahmadi-Nedushan, B. Prediction of elastic modulus of normal and high strength concrete using ANFIS and optimal nonlinear regression models. *Constr. Build. Mater.* **2012**, *36*, 665–673. [CrossRef]
12. EN 15804:2012+A2:2019 Sustainability of construction works—Environmental product declarations—Core rules for the product category of construction products. Available online: https://standards.iteh.ai/catalog/standards/cen/c98127b4-8dc2-48a4-9338-3e1366b16669/en-15804-2012a2-2019 (accessed on 17 February 2022).
13. Luo, R.; Cai, Y.; Wang, C.; Huang, X. Study of chloride binding and diffusion in GGBS concrete. *Cem. Concr. Res.* **2003**, *33*, 1–7. [CrossRef]

14. Sajedi, F.; Razak, H.A.; Bin Mahmud, H.; Shafigh, P. Relationships between compressive strength of cement–slag mortars under air and water curing regimes. *Constr. Build. Mater.* **2012**, *31*, 188–196. [CrossRef]
15. Goyal, A.; Palaia, I.; Ioannidou, K.; Ulm, F.-J.; van Damme, H.; Pellenq, R.J.-M.; Trizac, E.; Del Gado, E. The physics of cement cohesion. *Sci. Adv.* **2021**, *7*. [CrossRef] [PubMed]
16. Palomo, A.; Grutzeck, M.W.; Blanco, M.T. Alkali-activated fly ashes. *Cem. Concr. Res.* **1999**, *29*, 1323–1329. [CrossRef]
17. Palomo, A.; Krivenko, P.V.; Garcia-Lodeiro, I.; Kavalerova, E.; Maltseva, O.; Fernández-Jimenez, A.M. A review on alkaline activation: New analytical perspectives. *Mater. Constr.* **2014**, *64*, e022. [CrossRef]
18. Ünal, O.; Uygunoğlu, T.; Yildiz, A. Investigation of properties of low-strength lightweight concrete for thermal insulation. *Build. Environ.* **2007**, *42*, 584–590. [CrossRef]
19. Bogas, J.A.; de Brito, J.; Figueiredo, J.M. Mechanical characterization of concrete produced with recycled lightweight expanded clay aggregate concrete. *J. Clean. Prod.* **2014**, *89*, 187–195. [CrossRef]
20. Kurpińska, M.; Ferenc, T. Effect of porosity on physical properties of lightweight cement composite with foamed glass aggregate. In Proceedings of the ITM Web of Conferences, Guangzhou, China, 26–28 May 2017; Borys, M., Czyż, Z., Falkowicz, K., Kujawska, J., Kulisz, M., Szala, M., Eds.; Volume 15, p. 06005.
21. Rumsys, D.; Spudulis, E.; Bacinskas, D.; Kaklauskas, G. Compressive Strength and Durability Properties of Structural Lightweight Concrete with Fine Expanded Glass and/or Clay Aggregates. *Materials* **2018**, *11*, 2434. [CrossRef]
22. Dehdezi, P.K.; Erdem, S.; Blankson, M.A. Physico-mechanical, microstructural and dynamic properties of newly developed artificial fly ash based lightweight aggregate—Rubber concrete composite. *Compos. Part B Eng.* **2015**, *79*, 451–455. [CrossRef]
23. Al-Allaf, M.H.; Weekes, L.; Augusthus-Nelson, L.; Leach, P. An experimental investigation into the bond-slip behaviour between CFRP composite and lightweight concrete. *Constr. Build. Mater.* **2016**, *113*, 15–27. [CrossRef]
24. Khatib, J.; Hibbert, J. Selected engineering properties of concrete incorporating slag and metakaolin. *Constr. Build. Mater.* **2005**, *19*, 460–472. [CrossRef]
25. Hearn, E.J. *Mechanics of Materials 2: The Mechanics of Elastic and Plastic Deformation of Solids and Structural Materials Burlington*; Elsevier: Amsterdam, The Netherlands, 1997.
26. Aci Committee 318 and American Concrete Institute. *Building Code Requirements for Structural Concrete (ACI 318-19): An ACI Standard: Commentary on Building Code Requirements for Structural Concrete (ACI 318R-19)*; American Concrete Institute: Farmington Hills, MI, USA, 2019.
27. European Committee for Standardization. *Eurocode 2: Design of Concrete Structures—Part 1-1: General Rules and Rules for Buildings*; European Union: Brussels, Belgium, 2010; p. 225.
28. Zhu, R.; Alam, S.Y.; Loukili, A. An experimental investigation on the correlation between the aggregate size effect and the structural size effect. *Eng. Fract. Mech.* **2020**, *234*, 107101. [CrossRef]
29. Jin, L.; Yu, W.; Du, X.; Yang, W. Meso-scale simulations of size effect on concrete dynamic splitting tensile strength: Influence of aggregate content and maximum aggregate size. *Eng. Fract. Mech.* **2020**, *230*, 106979. [CrossRef]
30. Tzimopoulos, C.; Papadopoulos, K.; Evangelides, C.; Spyrides, A. Analytical solution of nonlinear Boussinesq equation. *Desalination Water Treat.* **2022**, *260*, 225–234. [CrossRef]
31. Cho, Y.S.; Kim, J.H.; Hong, S.U. Compressive Strength Prediction of Porous Concrete Using Nondestructive Tests. *J. Civ. Eng. Archit.* **2011**, *5*, 1053.
32. Hedjazi, S. Compressive Strength of Lightweight Concrete. In *Compressive Strength of Concrete*; IOP Publishing: Bristol, UK, 2020. [CrossRef]
33. Nath, P.; Sarker, P.K. Flexural strength and elastic modulus of ambient-cured blended low-calcium fly ash geopolymer concrete. *Constr. Build. Mater.* **2017**, *130*, 22–31. [CrossRef]
34. Mouna, Y.; Batikha, M.; Suryanto, B. Low Carbon Recycled Aggregate Concrete: Roles of Slag and Silica FumeIn: ZEMCH Network. In Proceedings of the 8th Energy Mass Custom Home International Conference, Dubai, United Arab Emirates, 26 October 2021; pp. 1063–1074.
35. Higgins, D. Sustainable concrete: How can additions contribute? In Proceedings of the Annual Technical Symposium, London, UK, 28 March 2006; The Institute of Concrete Technology: London, UK, 2006; pp. 1–6.
36. Holland, T.C. *'Silica Fume User's Manual' (PDF)*; Silica Fume Association and United States Department of Transportation Federal Highway Administration Technical Report FHWA-IF-05-016; U.S. Dept of Transportation/Federal Highway Administration: Washington, DC, USA, 2005.
37. Kosmatka, S.; Kerkhoff, B.; Panerese, W. *Design and Control of Concrete Mixtures*, 14th ed.; Portland Cement Association: Skokie, IL, USA, 2002.
38. Avallone, E.A.; Iii, T.B.; Sadegh, A. Cement, Mortar, and Concrete. 2007. Available online: https://www.accessengineeringlibrary.com/content/book/9780071428675/toc-chapter/chapter6/section/section194 (accessed on 26 November 2022).
39. Aligizaki, K.K. *Pore Structure of Cement-Based Materials*; CRC Press: Boca Raton, FL, USA, 2005; ISBN 9780429079313.
40. *C78/C78M-21*; Standard Test Method for Flexural Strength of Concrete (Using Simple Beam with Third-Point Loading). ASTM International: West Conshohocken, PA, USA, 2021.
41. Zhang, Z.; Qian, S.; Ma, H. Investigating mechanical properties and self-healing behavior of micro-cracked ECC with different volume of fly ash. *Constr. Build. Mater.* **2013**, *52*, 17–23. [CrossRef]
42. *BS EN 13055*; Lightweight Aggregates. British Standards Institution: London, UK, 2021.

43. Han, B.; Sun, S.; Ding, S.; Zhang, L.; Yu, X.; Ou, J. Review of nanocarbon-engineered multifunctional cementitious composites. *Compos. Part A Appl. Sci. Manuf.* **2015**, *70*, 69–81. [CrossRef]
44. Khalil, W.; Ahmed, H.; Hussein, Z. Behavior of high performance artificial lightweight aggregate concrete reinforced with hybrid fibers. In Proceedings of the MATEC Web of Conferences, Abu Dhabi, United Arab Emirates, 20–22 November 2018; Al-Attar, T.S., Al-Neami, M.A., AbdulSahib, W.S., Eds.; Volume 162, p. 02001.
45. Christidis, K.; Badogiannis, E.; Mintzoli, C. Flexural behaviour of pumice lightweight concrete reinforced with end-hooked steel fibres. *Structures* **2021**, *33*, 3835–3847. [CrossRef]
46. Xie, J.; Kou, S.-C.; Ma, H.; Long, W.-J.; Wang, Y.; Ye, T.-H. Advances on properties of fiber reinforced recycled aggregate concrete: Experiments and models. *Constr. Build. Mater.* **2021**, *277*, 122345. [CrossRef]
47. Zhao, M.; Zhao, M.; Chen, M.; Li, J.; Law, D. An experimental study on strength and toughness of steel fiber reinforced expanded-shale lightweight concrete. *Constr. Build. Mater.* **2018**, *183*, 493–501. [CrossRef]
48. Esmaeili, J.; Ghaffarinia, M.; Nodehi, M.; Gencel, O.; Shi, J.; Ozbakkaloglu, T. Mechanical and fractural characteristics of structural lightweight fiber reinforced concrete. *Struct. Concr.* **2022**, 1–20. [CrossRef]
49. Chinzorigt, G.; Lim, M.K.; Yu, M.; Lee, H.; Enkbold, O.; Choi, D. Strength, shrinkage and creep and durability aspects of concrete including CO2 treated recycled fine aggregate. *Cem. Concr. Res.* **2020**, *136*, 106062. [CrossRef]
50. Domagała, L. A Study on the Influence of Concrete Type and Strength on the Relationship between Initial and Stabilized Secant Moduli of Elasticity. *Solid State Phenom.* **2016**, *258*, 566–569. [CrossRef]
51. Zhang, M.-H.; GjØrv, O.E. Mechanical Properties of High-Strength Light weight concrete. *ACI Mater. J.* **1991**, *88*, 240–247.
52. Szydłowski, R.; Łabuzek, B. Experimental Evaluation of Shrinkage, Creep and Prestress Losses in Lightweight Aggregate Concrete with Sintered Fly Ash. *Materials* **2021**, *14*, 3895. [CrossRef]
53. Yam, A.S.-T.; Mindess, S. The effects of fibre reinforcement on crack propagation in concrete. *Int. J. Cem. Compos. Lightweight Concr.* **1982**, *4*, 83–93. [CrossRef]
54. Choi, W.-C.; Jung, K.-Y.; Jang, S.-J.; Yun, H.-D. The Influence of Steel Fiber Tensile Strengths and Aspect Ratios on the Fracture Properties of High-Strength Concrete. *Materials* **2019**, *12*, 2105. [CrossRef]
55. Pisello, A.L.; Castaldo, V.L.; Pignatta, G.; Cotana, F.; Santamouris, M. Experimental in-lab and in-field analysis of waterproof membranes for cool roof application and urban heat island mitigation. *Energy Build.* **2016**, *114*, 180–190. [CrossRef]
56. Alma'Aitah, M.; Ghiassi, B. Development of cost-effective low carbon hybrid textile reinforced concrete for structural or repair applications. *Constr. Build. Mater.* **2022**, *341*, 127858. [CrossRef]
57. Zhu, Y.; Zhang, Z.C.; Yang, Y.G.; Yao, Y. Measurement and correlation of ductility and compressive strength for engineered cementitious composites (ECC) produced by binary and ternary systems of binder materials: Fly ash, slag, silica fume and cement. *Constr. Build. Mater.* **2014**, *68*, 192–198. [CrossRef]
58. Şahmaran, M.; Bilici, Z.; Ozbay, E.; Erdem, T.K.; Yucel, H.E.; Lachemi, M. Improving the workability and rheological properties of Engineered Cementitious Composites using factorial experimental design. *Compos. Part B Eng.* **2013**, *45*, 356–368. [CrossRef]
59. Pakravan, H.R.; Latifi, M.; Jamshidi, M. Ductility improvement of cementitious composites reinforced with polyvinyl alcohol-polypropylene hybrid fibers. *J. Ind. Text.* **2014**, *45*, 637–651. [CrossRef]
60. Siad, H.; Alyousif, A.; Keskin, O.K.; Keskin, S.B.; Lachemi, M.; Sahmaran, M.; Hossain, K.M.A. Influence of limestone powder on mechanical, physical and self-healing behavior of Engineered Cementitious Composites. *Constr. Build. Mater.* **2015**, *99*, 1–10. [CrossRef]
61. Halvaei, M.; Jamshidi, M.; Latifi, M.; Ejtemaei, M. Experimental investigation and modelling of flexural properties of carbon textile reinforced concrete. *Constr. Build. Mater.* **2020**, *262*, 120877. [CrossRef]
62. Deng, M.; Dong, Z.; Zhang, C. Experimental investigation on tensile behavior of carbon textile reinforced mortar (TRM) added with short polyvinyl alcohol (PVA) fibers. *Constr. Build. Mater.* **2019**, *235*, 117801. [CrossRef]
63. Bhat, K.M.U.D.; Khan, M.Z. Effect of Steel Fibre Reinforcement on Early Strength of Concrete. *Int. J. Trend Sci. Res. Dev.* **2018**, *2*, 198–225. [CrossRef]
64. Moghaddam, F.; Hocking, D.; Jones, C.; Dingle, L. Investigation on the effect of low carbon, low shrinkage, high flexural strength envisia® concrete on industrial floor and pavement application. In Proceedings of the Australian Society for Concrete Pavements 5th Concrete Pavements Conference, Boral, Australia, 21–24 July 2019.
65. Olubanwo, A.O.; Karadelis, J.N.; Saidani, M.; Khorami, M.; Abbey, S.J. Investigation of intrinsic de-bonding in bonded concrete overlays: Material characterisation and numerical Study. *Eng. Solid Mech.* **2018**, *6*, 155–174. [CrossRef]
66. Abbey, S.J.; Eyo, E.U.; Oti, J.; Amakye, S.Y.; Ngambi, S. Mechanical Properties and Microstructure of Fibre-Reinforced Clay Blended with By-Product Cementitious Materials. *Geosciences* **2020**, *10*, 241. [CrossRef]
67. Abbey, S.J.; Ngambi, S.; Ganjian, E. Development of Strength Models for Prediction of Unconfined Compressive Strength of Cement/Byproduct Material Improved Soils. *Geotech. Test. J.* **2017**, *40*, 928–935. [CrossRef]
68. Abbey, S.J.; Eyo, E.U.; Okeke, C.A.; Ngambi, S. Experimental study on the use of RoadCem blended with by-product cementitious materials for stabilization of clay soils. *Constr. Build. Mater.* **2021**, *280*, 122476. [CrossRef]
69. Yang, W.J.; Li, Y. Mechanical Performance of the Different Structure Based on Shrinkage and Creep. *Appl. Mech. Mater.* **2013**, *405–408*, 1204–1207. [CrossRef]
70. Bažant, Z.P. Prediction of concrete creep and shrinkage: Past, present and future. *Nucl. Eng. Des.* **2001**, *203*, 27–38. [CrossRef]
71. Reed-Hill, R.E.; Abbaschian, R. *Physical Metallurgy Principles Boston*; Pws-Kent Pub: Boston, MA, USA, 1992.

72. Nevile, A.M. *Properties of Concrete*, 4th ed.; Longman: Harlow, UK, 1995.
73. Castel, A. Time-dependent behaviour of a class f fly ash-based geopolymer concrete. *Int. J. Res. Eng. Technol.* **2014**, *3*, 109–113.
74. Sprince, A.; Pakrastinsh, L.; Korjakins, A. Experimental Creep test on concrete made with montmorillonite Nano particles. In Proceedings of the 8th International Conference: Concrete in the Low Carbon Era, Dundee, UK, 9 July 2012.
75. Lambert, G. Properties and Behaviour of Structural Lightweight (Lytag-Sand) Concrete. Ph.D. Thesis, University of Sheffield, Sheffield, UK, 1982; pp. 1–304.
76. Lytag. *Technical Manual—Section 4 Design Guidance for Lytag LWAC (Concrete)*; Lytag Limited: London, UK, 2017.
77. Robalo, K.; Soldado, E.; Costa, H.; Carvalho, L.; do Carmo, R.; Júlio, E.N.B.S. Durability and Time-Dependent Properties of Low-Cement Concrete. *Materials* **2020**, *13*, 3583. [CrossRef]
78. Safiuddin; Salam, M.; Jumaat, M.Z. Effects of recycled concrete aggregate on the fresh properties of self-consolidating concrete. *Arch. Civ. Mech. Eng.* **2011**, *11*, 1023–1041. [CrossRef]
79. OBE, R.K.D.; de Brito, J.; Silva, R.V.; Lye, C.Q. *Chapter 9: Deformation of Concrete Containing Recycled Concrete AggregateIn: Sustainable Construction Materials: Recycled Aggregates*; Woodhead Publishing: Sawston, UK, 2019; pp. 283–363.
80. Lopez, M. *Creep and Shrinkage of High-Performance Lightweight Concrete: A Multi Scale Investigation*; Doctoral Dissertation Georgia Institute of Technology: Atlanta, GA, USA, 2005.
81. Lopez, M.; Kahn, L.F.; Kurtis, K.E. High-strength self-curing low-shrinkage concrete for pavement applications. *Int. J. Pavement Eng.* **2010**, *11*, 333–342. [CrossRef]
82. Mazloom, M.; Mahboubi, F. Evaluating the settlement of lightweight coarse aggregate in self-compacting lightweight concrete. *Comput. Concr.* **2017**, *19*, 203–210. [CrossRef]
83. Wendling, A.; Sadhasivam, K.; Floyd, R.W. Creep and shrinkage of lightweight self-consolidating concrete for prestressed members. *Constr. Build. Mater.* **2018**, *167*, 205–215. [CrossRef]
84. Nochaiya, T.; Wongkeo, W.; Chaipanich, A. Utilization of fly ash with silica fume and properties of Portland cement–fly ash–silica fume concrete. *Fuel* **2010**, *89*, 768–774. [CrossRef]
85. Samad, S.; Shah, A.; Limbachiya, M.C. Strength development characteristics of concrete produced with blended cement using ground granulated blast furnace slag (GGBS) under various curing conditions. *Sādhanā* **2017**, *42*, 1203–1213. [CrossRef]
86. Liu, Y.; Zhou, X.; Lv, C.; Yang, Y.; Liu, T. Use of Silica Fume and GGBS to Improve Frost Resistance of ECC with High-Volume Fly Ash. *Adv. Civ. Eng.* **2018**, *2018*, 7987589. [CrossRef]
87. Premkumar, R.; Hariharan, P.; Rajesh, S. Effect of silica fume and recycled concrete aggregate on the mechanical properties of GGBS based geopolymer concrete. *Mater. Today Proc.* **2022**, *60*, 211–215. [CrossRef]
88. Vollpracht, A.; Soutsos, M.; Kanavaris, F. Strength development of GGBS and fly ash concretes and applicability of fib model code's maturity function—A critical review. *Constr. Build. Mater.* **2018**, *162*, 830–846. [CrossRef]
89. Candelaria, M.D.E.; Kee, S.-H.; Lee, K.-S. Prediction of Compressive Strength of Partially Saturated Concrete Using Machine Learning Methods. *Materials* **2022**, *15*, 1662. [CrossRef]
90. Yehia, S.; Farrag, S.; Helal, K.; Shahinaz, S. Effects of Fly Ash, Silica Fume, and Ground Granulated Blast Slag on Properties of Self Compacting High Strength Lightweight Concrete. *GSTF J. Eng. Technol. (JET)* **2015**, *3*, 1–9. [CrossRef]
91. Gandomi, A.H.; Roke, D.A. Assessment of artificial neural network and genetic programming as predictive tools. *Adv. Eng. Softw.* **2015**, *88*, 63–72. [CrossRef]
92. Driscoll, T.A. *Learning Matlab*; Society for Industrial and Applied Mathematics: Philadelphia, PA, USA, 2009.
93. Swamy, R.; Lambert, G. The microstructure of Lytag aggregate. *Int. J. Cem. Compos. Light. Concr.* **1981**, *3*, 273–282. [CrossRef]